

## *Results and Discussion*

## CHAPTER IV

### RESULTS AND DISCUSSION

This chapter details the outcomes of the studies carried out for design and develop an air-assisted electrostatic sprayer nozzle for coconut palms. The section systematically describes the findings from preliminary studies, development procedures of the high voltage electric circuit, spraying nozzle and air-assistance blower assembly. Through comprehensive analysis and testing, the chapter aims to demonstrate the sprayer's effectiveness and potential applications, providing a foundation for future advancements in electrostatic spraying technology.

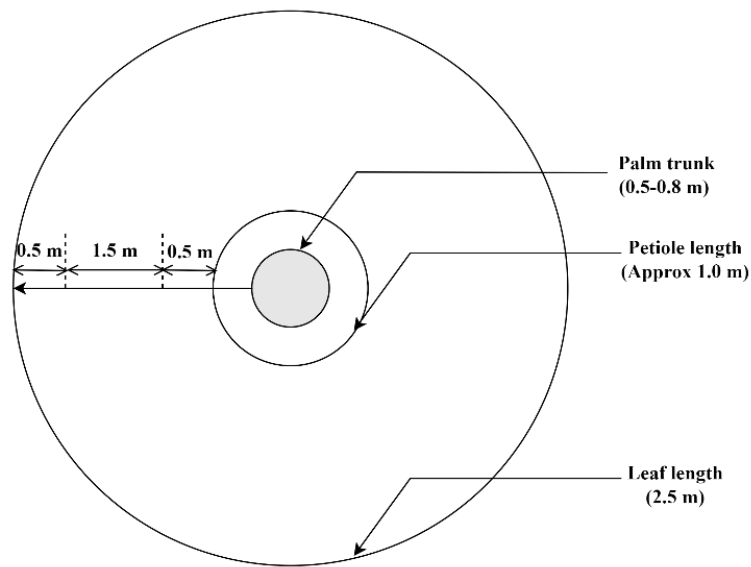
#### 4.1 PALM ARCHITECTURE

The morphological parameters of the coconut palm including the height, leaf diameter, and angle of leaf inclination were measured in the field and recorded. The observations were taken from the 30 coconut palms at the instructional farm, KCAET, Tavanur and given in Table 2 and details are given in appendix I.

**Table 2. Palm architecture**

Sl. No.	Parameter	Minimum	Maximum	Mean	SD
1.	Height of Coconut palm, m	6.56	12.5	9.12	1.88
2.	Length of leaf, m	1.98	4.38	3.54	0.74
3.	Canopy diameter, m	3.96	8.76	7.09	1.45
4.	Angle of leaf orientation, degree	36	82	57.47	12.32

The average height of the palm trees was observed as  $9.12 \pm 1.88$  m. For the preliminary study on electrostatic spraying, coconut palms of short to medium height have been selected for the optimal testing conditions. The average length of leaf (fronds) and canopy diameter was recorded as 3.54 m and 7.09 m respectively. The angle of leaf orientation relative to the vertical axis was observed between 36° to 82°. It was found to be significantly influenced by the leaf's age. As the leaf matures, its inclination gradually increases, detaches from the trunk and falls off.



**Figure 14. Palm leaf canopy**

As shown in the Figure 14, the palm leaf frond measures 3.5 m in total length, comprising a 1 m petiole and a 2.5 m leaf-bearing portion that requires spraying. Covering the entire 2.5 m spray swath with multiple nozzles would increase the unit's weight, leading to practical feasibility issues. Therefore, a single-nozzle unit with multiple passes would be more suitable. The leaf-bearing portion can be divided into three sections: a central, relatively straight 1.5 m section; a 0.5 m slanted portion with smaller, closely packed leaflets at the open end; and another 0.5 m portion near the base with broader, longer, and more widely spaced leaflets. The central 1.5 m portion, which contains the majority of leaves highly susceptible to pest attacks, should receive thorough spray coverage in one or multiple passes for effective pest control.

#### 4.2 DEVELOPMENT OF ELECTROSTATIC SPRAYER

The electrostatic sprayer for coconut palms primarily consists of high voltage DC generation unit, nozzle unit, liquid delivery unit, and air-assistance unit. The subsystem of each major components and their constructional details are discussed in detail below.

#### **4.2.1 Development of high voltage DC power supply**

The fabricated unit of HVDC module consists of power source, Line Output (LOPT) or flyback transformer, Pulse Width Modulator (PWM), MOSFET switching circuit, capacitors, ON-OFF switch, and electrode assembly. The details of each component are discussed in the following sections.

##### *4.2.1.1 High voltage generation*

The developed high voltage system based on LOPT transformer (Figure 15) and MOSFET was efficient enough to produce voltage up to +11 kV DC with an input supply ranging between 3 and 7 V. The power source for the developed unit comprised four rechargeable Lithium-ion (Li-ion) batteries each with an open circuit voltage of 3.7 V (at full charge) and capacity of 5000 mAh connected in parallel ( Figure 16). The initial electric signals from the power source were then given to the LOPT or flyback transformer (1010A) through an oscillator circuit, which was a IRFZ44E MOSFET. The LOPT 1010A is a step-up transformer designed with less no of turns in the primary windings compared to the secondary windings. It operates on the principle of electromagnetic induction, where a changing current in the primary winding induces a high voltage in the secondary winding. The primary circuit of the LOPT transformer has three tapping positions two at each end and one at the center.

A MOSFET generally has three pins namely gate, drain and source denoted as 'G', 'D', and 'S' respectively as shown in Figure 17. The negative terminal of the battery was given to the gate of the MOSFET. An electrolytic capacitor of 25 V DC, 2.2 uF was connected in parallel at the input side of the oscillator (MOSFET) to filter the electric signals from the source. The drain pin of the MOSFET was connected to the one end of the (bottom) primary windings of the LOPT transformer and the source pin was connected to the other end (upper middle) of the primary circuit through a series connection of 150  $\Omega$  resistance. The middle tapping point of the LOPT transformer was wired to the positive terminal of battery assembly. The IRFZ44E MOSFET (Figure 17) is turned on and off rapidly, these rapid switching of the MOSFET creates alternating magnetic fields in the transformer core, which in turn leads to the generation of a high voltage generation in the secondary windings of the

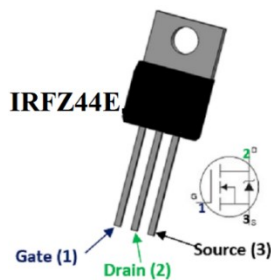
transformer due to the turn's ratio between the primary and secondary windings. The output of the transformer was given to the high voltage electrode for the electrostatic induction charging of the spray droplets. A series arrangement of seven high voltage polymer capacitors (2000 V DC, 22 nF) were connected across the transformer output to handle accidental loading and as a filter the noise.



**Figure 15. LOPT 1010A transformer    Figure 16. Li-ion rechargeable batteries**

#### 4.2.1.2 Pulse Width Modulator (PWM)

The high voltage DC circuit was designed to acquire different output voltages with the help of a Pulse Width Modulator (PWM) of 0 to 30 V as shown in Figure 18. The PWM connects in between the MOSFET and power source, regulates the input voltage to the MOSFET. As a result, the output of HVDC system can vary anywhere between 1 kV to 11 kV with a maximum current of 30  $\mu$ A.

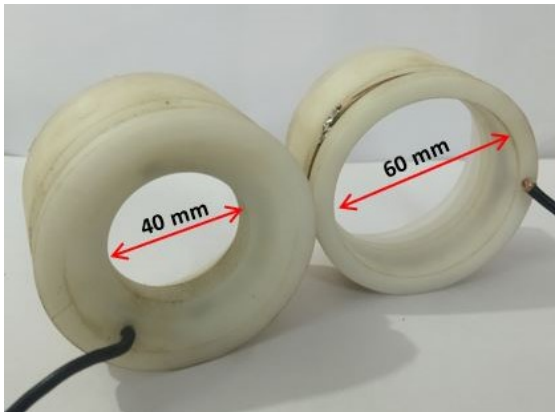


**Figure 17. IRFZ44E MOSFET    Figure 18. Pulse Width Modulator (PWM)**

#### 4.2.1.3 Development of high voltage electrode assembly

The effect of the diameter of electrodes and their horizontal positions with respect to the spray nozzle was studied using three embedded electrodes of diameters,

40, 60, and 90 mm denoted as E4, E6, and E9 respectively. All the electrodes were made of 4.3 mm thick copper wire. The E9 electrode was decided to place outside the spray gun with proper insulation. Whereas the E4 and E6 electrodes are decided to place inside the spray gun with proper electrode carrier sleeves as shown in Plate 3. The electrode carrier sleeves for electrodes E4 and E6 were fabricated using cast nylon (average dielectric strength:  $28.6 \text{ kV} \cdot \text{mm}^{-1}$ ), which has an excellent electrical insulation property. The external diameters of these sleeves were designed to ensure a close-fitting within the nozzle-air blower conduit, allowing for easy replacement. The sleeves are capable of sliding within the conduit, enabling adjustable horizontal positioning of the electrodes E4 and E6 relative to the droplet formation zone as required. The electrode carrier sleeve for E4 has an internal diameter of 40 mm at the intake and 76 mm at the exit side, while the electrode carrier sleeve for E6 has an internal diameter of 60 mm at the intake and 76 mm at the exit side. This design of the carrier sleeves ensures complete insulation of the high-potential electrodes, thereby preventing accidental human contact with the high-voltage electrode. In addition, this design protects the electrode material from corrosion caused by chemical reactions and environmental factors.



(a)



(b)

**Plate 3. Electrodes with carrier sleeves (a) 40 and 60 mm diameter electrodes (b) 90 mm diameter electrode**

#### 4.2.1.4 Working of the HVDC power system

The high-voltage DC system was powered by four Lithium-ion batteries, each with an open circuit voltage of 3.7 V, connected in parallel. This parallel configuration ensures a stable voltage supply while increasing the overall current capacity, thereby enhancing the system's runtime and power delivery. The initial electrical signal from the batteries was filtered using a 25 V DC, 2.2  $\mu\text{F}$  capacitor before being fed to the LOPT (flyback transformer 1010A) through an IRFZ44E MOSFET. The MOSFET acts as an electronic switch to control the current flow through the step-up transformer. When the MOSFET is on, it allows current to flow through the transformer's primary winding, creating a magnetic field. When the MOSFET switches off, the collapsing magnetic field in the primary winding induces a high voltage in the secondary winding. This induced high voltage is then connected to the electrode for electrostatic induction charging of spray droplets. To filter the signals and handle accidental loading, a series arrangement of 2000 V, 0.022  $\mu\text{F}$  capacitors were connected across the transformer's output. The negative terminal of the transformer output was connected to an embedded electrode positioned at the spray nozzle, while the positive terminal was connected to the fertilizer-water tank. As the liquid is sprayed out from the nozzle and flows near the high-voltage electrode, the circuit is completed, and the droplets are charged by electrostatic induction.

#### 4.2.2 Development of spray nozzle

The atomization of spray liquid was achieved by a solid cone hydraulic nozzle made of Acrylonitrile Butadiene Styrene (ABS) with an orifice diameter of 0.5 mm with an operating pressure and discharge range of 3 to 5  $\text{kg}\cdot\text{cm}^{-2}$  and 4.7 to 7.5  $\text{L}\cdot\text{h}^{-1}$  respectively. The rear end of the nozzle was threaded to perfectly fit the threads of nozzle holder, which was made of cast nylon. This arrangement of nozzle as shown in Plate 4 secures the nozzle from being displaced or splash away during the operation. The nozzle assembly was concentrically installed inside a conduit made of cast nylon by means of PVC fittings. The cast nylon conduit with stepping, houses both the nozzle and the air-blower assembly (EDF). The nozzle assembly was inserted at the front end of the conduit having an internal diameter (ID) of 80 mm whereas the air-blower

assembly (EDF) was installed at the rear end of the conduit having an internal diameter of 70 mm. The liquid delivery from the diaphragm pump to the nozzle was made using 10 m long polyurethane hose (10 mm OD and 6.5 mm ID) and compression fitting connectors.



**Plate 4. Arrangement of spray nozzle inside the spray gun**

#### **4.2.3 Development of liquid delivery unit**

A self-priming double stage diaphragm pump featuring a cutoff pressure of  $10.5 \text{ kg}\cdot\text{cm}^{-2}$  and an open flow of  $10 \text{ L}\cdot\text{min}^{-1}$ , powered by a 12 V DC battery was selected for the liquid delivery. The delivery from the pump was rerouted back to the tank through a dual-channel differential valve to ensure optimal hydraulic pressure at the nozzle. This rerouted flow is utilized to maintain continuous agitation of the spray solution throughout the operation. A pressure gauge was provided to accurately measure and monitor the operating pressure of the system, ensuring it remains within the desired range for optimal performance.

#### **4.2.4 Design of battery-operated air assistance unit**

The design or selection of suitable air-assistance unit were done based on the theoretical requirement of air flow volume and air flow velocity to cover 1 m spraying swath of the developed nozzle. From these calculations, the thrust and power requirement of the fan unit have been derived, which ensures that the fan unit aligns the specified parameters.



#### 4.2.4.1 Theoretical analysis of air volume and air flow

The sprayer unit was decided to carry by an individual in the field with the backpack and long telescopic pole (8 m) fitted with the spray gun at the upper middle. The speed of operation with the sprayer was then taken as the average walking speed of a man ( $0.5 \text{ m}\cdot\text{s}^{-1}$ ). Considering the tall nature of coconut palm, it was assumed that the spray gun should be at a maximum of 1.5 m below the lower palm leaf ( $H_1$ ) and the coconut palm canopy height was taken as 1.5 m ( $H_2$ ). The spray swath of the nozzle at 1.5 m position was observed as 800 mm ( $L$ ). The diameter of the fan blade was taken as 70 mm as it must be smaller than the width of spray gun outlet (9 cm).

According to the principle of displacement of air volume, the required airflow volume is,

$$Q_{required} = vd (H_1 + H_2)K_1$$

Substituting the values of each parameter in the above equation, the required air volume was calculated as  $0.867 \text{ m}^3\cdot\text{s}^{-1}$ .

According to the principle of terminal velocity of air flow, the required airflow velocity is,

$$V_1 = \frac{V_2 L}{K_2 d}$$

The spraying in orchard canopy (pear) with air assisted sprayers was effective when the terminal air flow velocity was in the range of  $2.7$  to  $3.18 \text{ m}\cdot\text{s}^{-1}$  (Shi *et al.* 2022). Miao *et al.* (2023) was taken the terminal air velocity as  $2$  to  $4 \text{ m}\cdot\text{s}^{-1}$  for the design of air-assisted system for high stalk crops. From the literature reviews, the terminal velocity ( $V_2$ ) was taken as  $3.0 \text{ m}\cdot\text{s}^{-1}$ . Substituting the values in the equation,  $V_1$  is determined as  $14.80 \text{ m}\cdot\text{s}^{-1}$ , which found to be on par with the results obtained with Xue *et al.*, 2023 (air assisted electrostatic sprayer for citrus orchard with 1 m spraying distance,  $0.50 \text{ m}\cdot\text{s}^{-1}$  forward speed, and  $V_1$ :  $10 \text{ m}\cdot\text{s}^{-1}$ ).

Hence, from the theoretical analysis, the required air assisted system should be capable of generating an airflow volume of  $0.867 \text{ m}^3\cdot\text{s}^{-1}$  and velocity of  $14.80 \text{ m}\cdot\text{s}^{-1}$  at

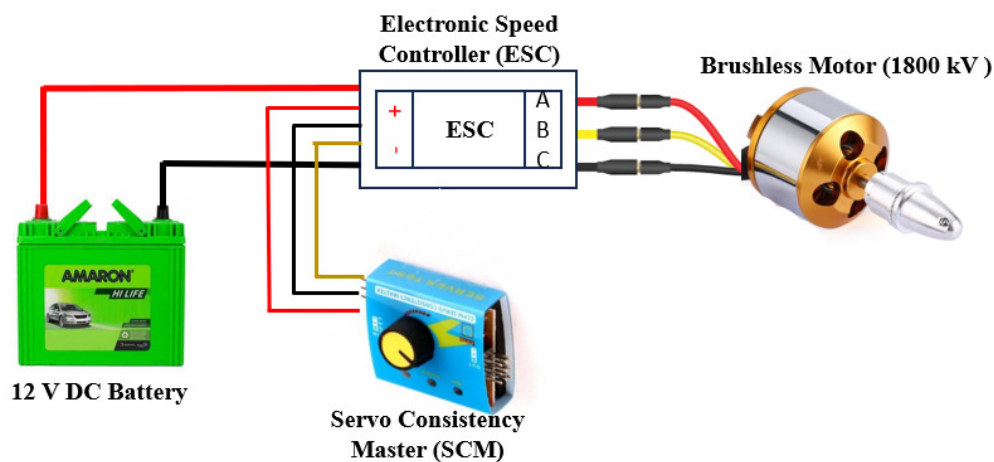
the fan outlet. By applying the equation of continuity, the diameter required for the fan was determined as 27.30 cm, which were found to be significantly larger than the dimensions of the spray gun (90 mm diameter), and it may also add unnecessary weight to the unit. This is particularly problematic because the narrower upper middle diameter of the telescopic pole must support the weight of the spray gun. To address this issue, a fan unit with a high thrust-to-diameter ratio would be a more appropriate solution, as it would provide the necessary air flow velocity, without contributing excessive weight or requiring a larger diameter.

#### 4.2.4.2 Selection of air-assistance unit or Electric Ducted Fan (EDF)

Ducted fans are capable of generating several fold static thrust for a given diameter when compared to open propeller fans (Urban *et al.*, 2023; Zhao *et al.*, 2022). The duct aids to accelerate the air flow and result in more efficient thrust generation. The most important step in the design of an EDF is the calculation of desired thrust. This parameter serves as a fundamental metric upon which all other design considerations are based and also for evaluating the performance capabilities of the system. Accurate assessment of required thrust determines the specification of power source (motor), duct configurations, geometry of blades and also aids in the identification of most effective operating points and adjusting parameters accordingly to maximize overall system efficiency. The EDF should produce sufficient thrust essential for the payload capacity. The EDF for the air assisted system is operating in a stationary position, hence the conditions for the static operation were applied to calculate the thrust and power requirement. Under static operating condition, the forward velocity is zero.

On viewing facts of weight reduction, the diameter of the ducted fan was assumed as 70 mm. By substituting the values of required airflow volume ( $Q_e = Q_{required} = 0.867 \text{ m}^3 \cdot \text{s}^{-1}$ ), velocity ( $V_e = V_1 = 14.80 \text{ m} \cdot \text{s}^{-1}$ ), and fan diameter in the equations, the minimum required mass flow rate (M) and thrust (T) of the ducted fan was estimated as  $1.05 \text{ kg} \cdot \text{s}^{-1}$  and 1.62 kgf or 16.20 N respectively. The power required for the fan was determined as 114.99 W. Assuming the fan system and motor efficiency

as 80 and 85 per cent respectively, the minimum power required for the motor was found as 169.11 W, which can be approximated as 170 W. Commercially available brushless motors typically smaller and lighter are capable of achieve higher speed make them suitable for applications demanding high performance and precise control. They are capable of producing substantial thrust even with smaller propellers. Brushless motors paired with electronic speed controllers (ESCs) and Servo Consistency Master (SCM) as shown in Figure 19, provide advance speed and direction control.



**Figure 19. Circuit diagram of Electric Ducted Fan (EDF)**

#### **4.2.5 Adjustable spray extension pole**

A carbon fiber pole measures 8 meters in length, with a tapered diameter to provide optimal strength and ease of use. The overall weight of the pole is 1450 g, which highlights its lightweight construction, a key feature made possible by the use of carbon fiber. Carbon fiber is known for its high strength-to-weight ratio, making the pole both robust and easy to handle.

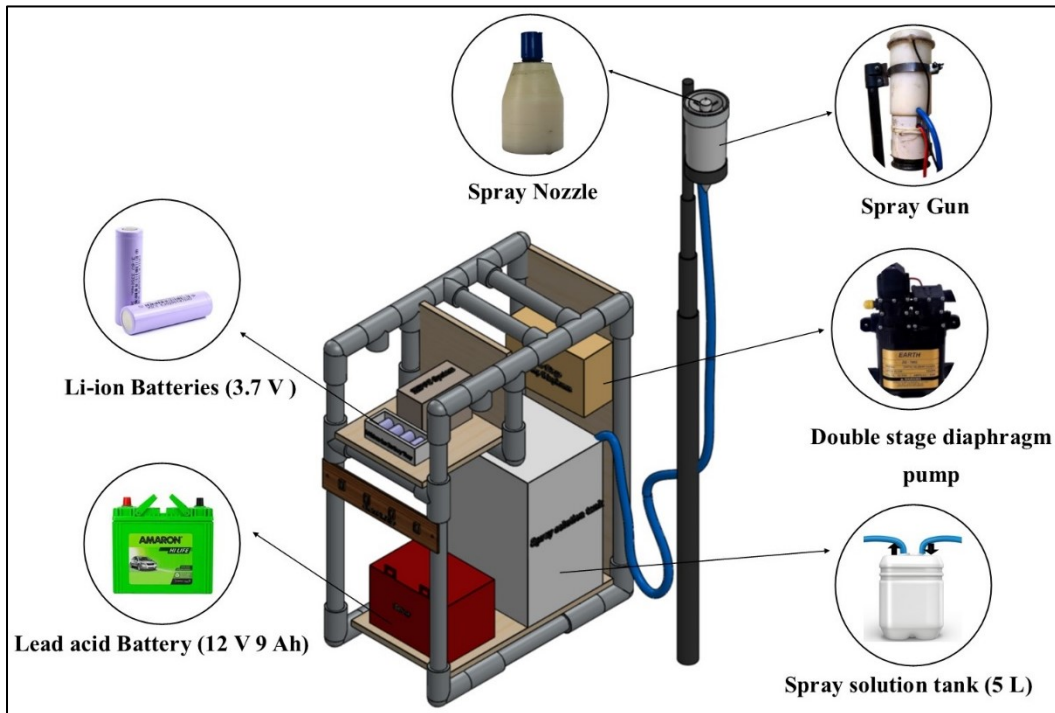
The bottom of the pole has a larger diameter of 32 mm to ensure stability and support, gradually narrowing to a smaller diameter of 22 mm at the upper middle to reduce weight and enhance maneuverability. This design balances durability and user comfort, making it suitable for extended use without causing fatigue. The spray gun was mounted at the upper middle end of the telescopic pole as shown in Plate 5. It is securely fixed to ensure consistent performance and precise application.

#### 4.2.6 Backpack frame

Carrying the pump assembly, battery, components of the HVDC generation system, and the speed control unit of the EDF while operating the sprayer in the field can be a challenging and exhausting task. This cumbersome process can significantly impact the operator's performance and reduce the overall efficiency of the spraying operation. To address this issue, a lightweight backpack frame was designed to house these components during field operations as shown in Plate 6. The frame was constructed using 25 mm PVC pipes, with the compartments and base made from 3 mm thick plywood sheets. This design ensures durability and stability while minimizing the overall weight, enhancing the operator's comfort and effectiveness.

The overall dimensions of the frame were  $404 \times 367 \times 239$  mm and weighted about 8.5 kg. The entire frame structure was divided lengthwise into two compartments, with the right compartment being wider than the left. The wider right compartment housed the spray solution tank of 5 L capacity, pump, valve, and pressure gauge. The left compartment was further subdivided horizontally into two sections: the lower left section housed the 12 V battery, while the upper left section contained the components of the HVDC generation unit and the speed control unit of the EDF. The components were securely positioned in their respective locations either by bolting them in place or by using appropriate adhesives. This ensures that each component is firmly anchored, preventing any movement or shifting during operation.

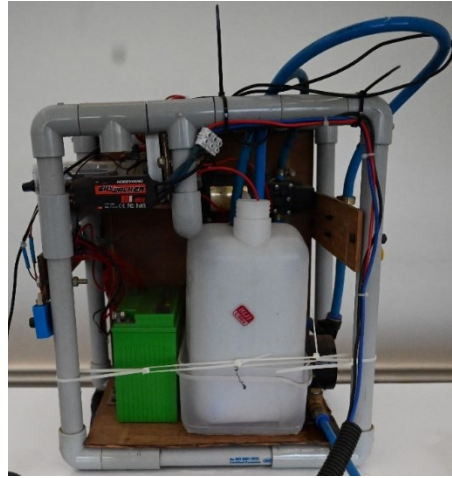
Three ON-OFF switches for controlling the operations of the EDF, HVDC system, and pump were mounted on the left-hand side of the frame to facilitate ease of operation in the field. This strategic placement allows the operator to manage the different systems efficiently while on the move. The operator can comfortably carry the backpack on their shoulders and, with the telescopic pole with spraying attachment held in their right hand, control the various functions using their left hand. This setup ensures that the operator can perform all necessary tasks with minimal effort and optimal control, enhancing both comfort and operational efficiency. The CAD of the developed prototype was given in Figure 20.



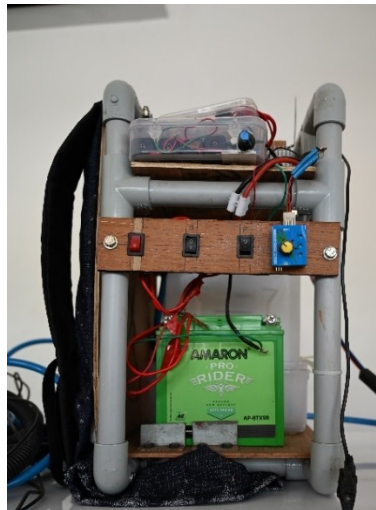
**Figure 20. CAD of air assisted electrostatic sprayer for coconut palms**



**Plate 5. Spray gun mounted at the top end of telescopic pole**



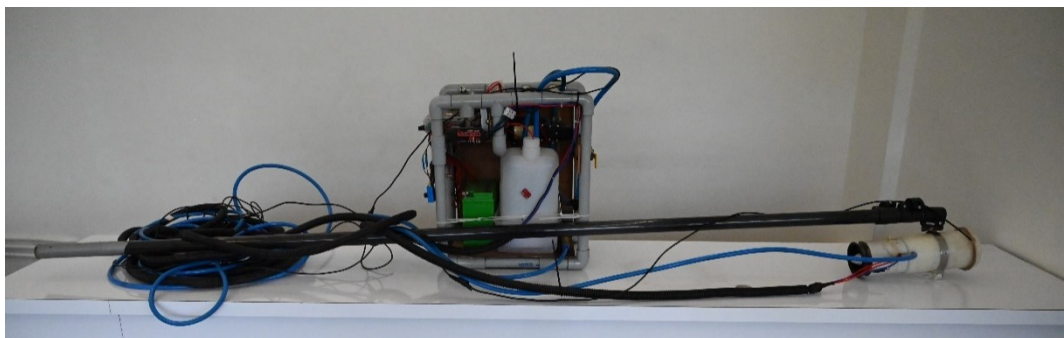
(a)



(b)



(c)



(d)

**Plate 6. Developed backpack structure for the sprayer**

**Table 3. Specification of the developed prototype**

Sl. No.	Components	Specifications
1.	Spray gun	: Length: 280 mm Diameter: 90 mm
	a. Adjustable spray extension pole	: Length: 8 m Weight: 1450 g
	b. Spray nozzle	: Type: Hydraulic pressure swirl Orifice diameter: 0.5 mm Diameter: 70 mm No. of blades: 12
	c. EDF unit	: Motor type: A2212-BLDC (kV1800) Operating voltage: 7.5 to 25 V DC ESC: UBEC 80 A
	d. Charging electrode	: Material: 43 mm dia Copper wire Diameter: 90 mm Dimension: 404 × 367 × 239 mm
2.	Backpack assembly	: Overall weight: 8.5 kg Material: CPVC 25 mm pipe outer dia.
	a. Tank	: Material: PVC Capacity: 5 L Topology: Resonant flyback transformer
	b. HVDC system	: Oscillator: IRFZ44N Power MOSFET Input voltage: 3 to 9 V DC Output voltage: 1 kV to 12 kV DC
	c. Battery	: 12 V 9 Ah Lead acid battery High pressure diaphragm (12V DC)
	d. Pump	: Max. current input: 6 A Max. pressure: 10 kg·cm <sup>-2</sup>

---

	Max. Discharge: 10.5 L·m <sup>-1</sup>
e. Liquid delivery	Material: polyurethane
hose	: Length: 10 m
	Internal diameter: 10 mm

---

### 4.3 LABORATORY EXPERIMENTS

The major results and conclusions derived from the laboratory experiments on Charge-to-Mass Ratio, electrode voltage, diameter and position of electrode with respect to the nozzle and droplet spectrum are discussed below.

#### 4.3.1 Measurement of Charge-to-Mass Ratio (CMR)

The effectiveness of the developed electrostatic induction charging system was analysed with Faraday cage apparatus. The operating conditions viz., electrode position relative to the nozzle (radial and horizontal), and the voltage were also optimized under indoor conditions. The charge carrying capacity of the optimized electrode-voltage composition was also determined.

##### 4.3.1.1 *Effect of voltage on CMR*

The effect of radial distance of the induction electrode on CMR was graphically represented in Figure 21 and Figure 22. The measurements were taken at 1 m and 2 m vertical distance between the Faraday cage and spray gun. The current readings for electrode voltages of 4 kV and 5 kV were observed to be zero. This could be attributed to insufficient droplet charging, induced charge on the droplets was of such low magnitude that it dissipated quickly as the droplets travelled even a short distance through the air. Therefore, further measurements were conducted at higher electrode potentials including 6, 7, 8, 9, and 10 kV. For all the radial and horizontal positions of the electrode, the CMR is increasing with the applied voltage with the highest value at 10 kV electrode voltage, followed by 9 kV. The maximum CMR of 3.61 mC·kg<sup>-1</sup> was obtained at 10 mm horizontal position with 90 mm diameter electrode, followed by the 3.45 mC·kg<sup>-1</sup> at 9 kV with the similar operating conditions. The minimum CMR values was observed at 6 kV electrode potential for all the operating conditions. The value of



CMR is found to decrease as the distance between the Faraday cage and spray gun increased. However, electrode potentials of 9 and 10 kV were able to maintain sufficient CMR levels of 1.57 and 1.27 mC·kg<sup>-1</sup> respectively up to a target distance of 2 meters.

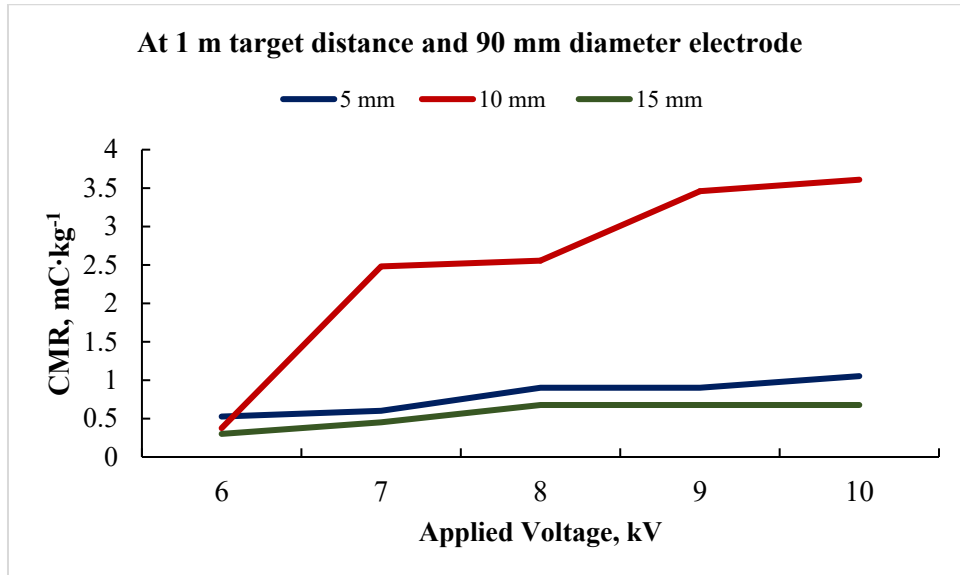
#### *4.3.1.2 Effect of horizontal distance of induction electrode on CMR*

The effect of radial distance of the induction electrode on CMR is graphically represented in Figure 23. All the three electrodes were positioned at 5, 10 and 15 mm in front of the nozzle. It was observed from the graph, that for all the three electrodes, the CMR increases as the electrode shifts from 5 to 10 mm moving towards the front of the nozzle tip. However, the further increase in horizontal distance from 10 to 15 mm shows a reduction in the CMR. It can be concluded that, across all the readings, the maximum charge induction was observed at a position near the droplet formation zone.

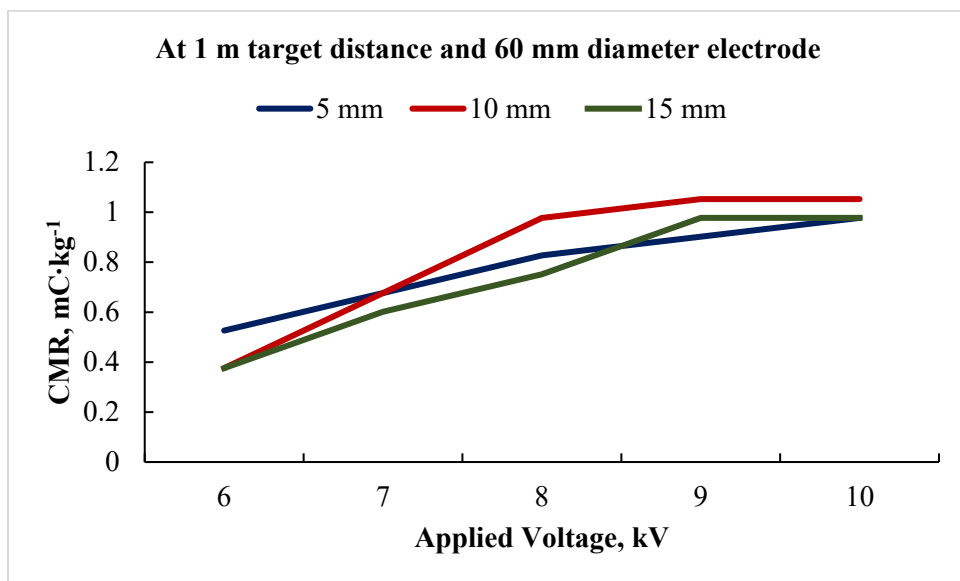
#### *4.3.1.3 Effect of diameter of induction electrode on CMR*

The effect of radial distance of the induction electrode on CMR is graphically represented in Figure 23. The voltage increase was clearly marked at the 10 mm electrode position with the 90 mm diameter electrode. The 60 mm diameter electrode, however showed lower CMR values compared to the 40 and 90 mm electrodes. Although, 40 mm diameter electrode produced notable CMR values, the reduction in cross-sectional area caused by the electrode carrier sleeve increased resistance to airflow. This restricted flow path resulted in shorter droplet travel distances and led to greater droplet deposition inside the spray gun. Over extended operation, this droplet buildup on the electrode carrier sleeve eventually caused dripping. The issue was worsened as the spray gun was held vertically, as the dripping droplets could lead to short-circuiting of the motor in the EDF. With the 60 mm diameter electrode, this problem was rarely observed, though its CMR was relatively insufficient. The 90 mm diameter electrode provided adequate CMR values with no droplet dripping, as it was positioned on the outer side of the spray gun. However, the main issue with this electrode was electrode-wetting, caused by the reverse movement of positively charged

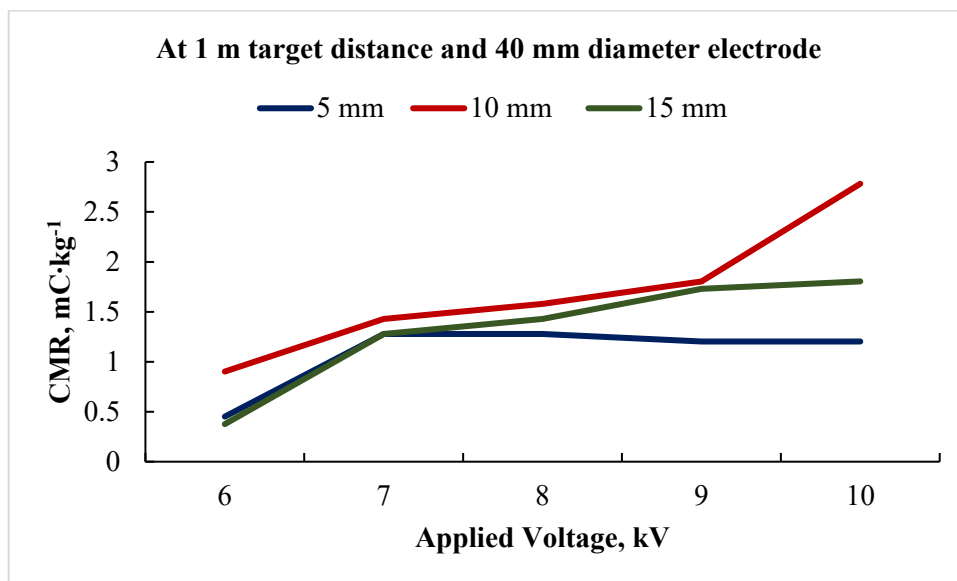
droplets toward the negatively charged electrode. This problem can be effectively managed by providing proper insulation to the electrode.



(a)

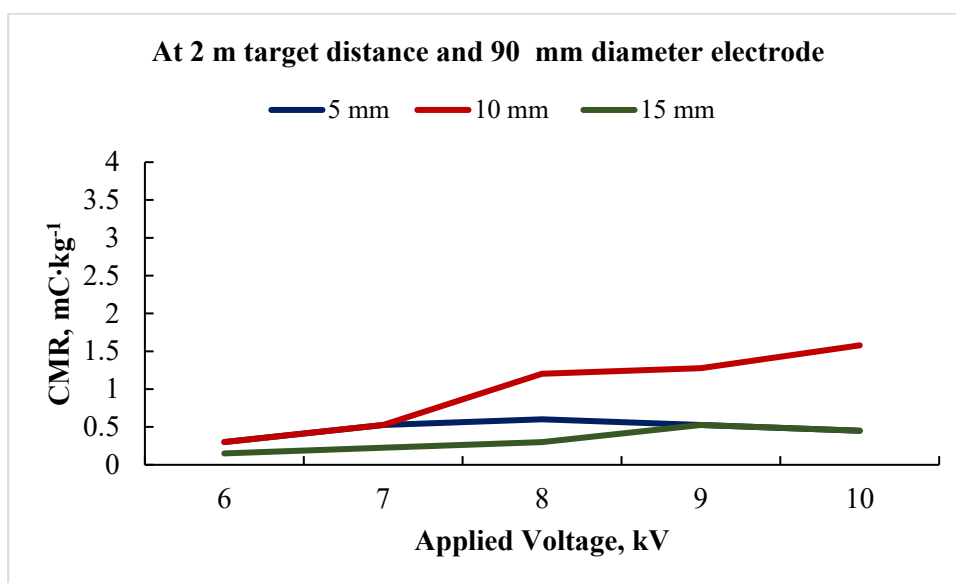


(b)

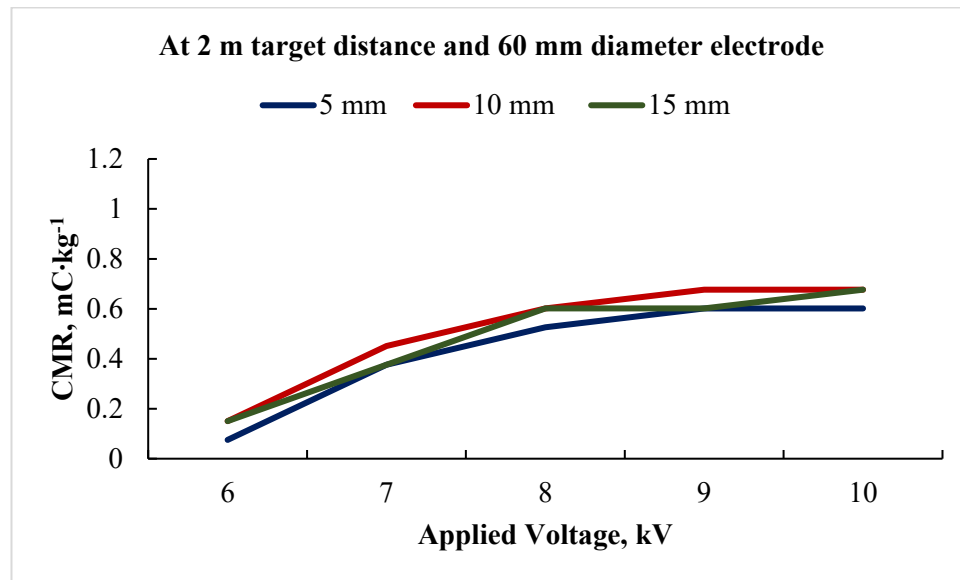


(c)

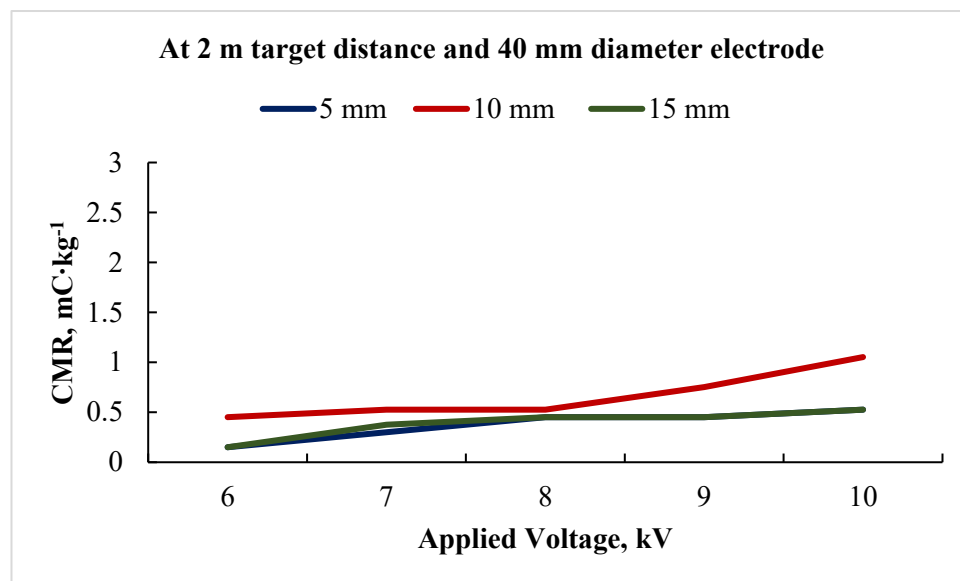
**Figure 21. Effect of applied electrode voltage on CMR at 1 m vertical distance**



(a)

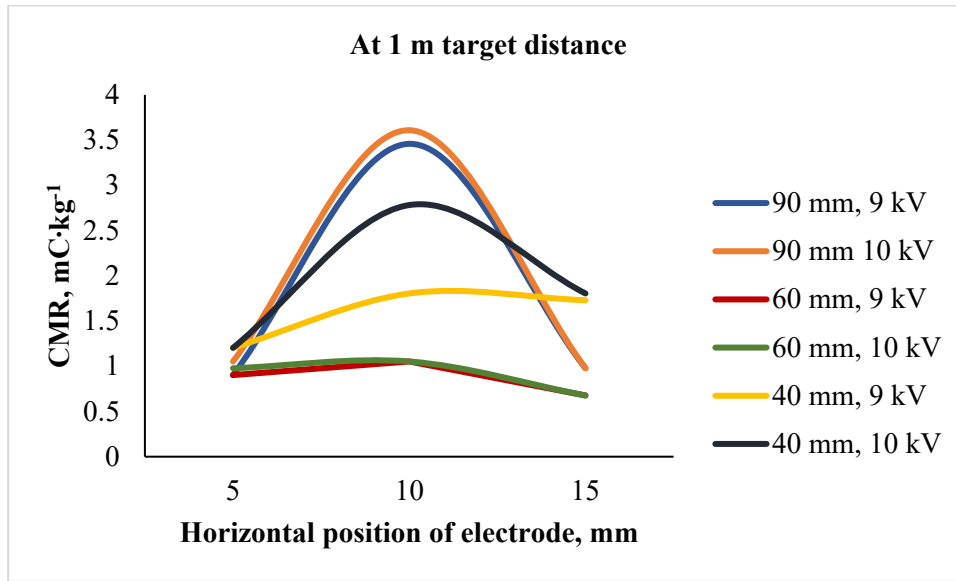


(b)

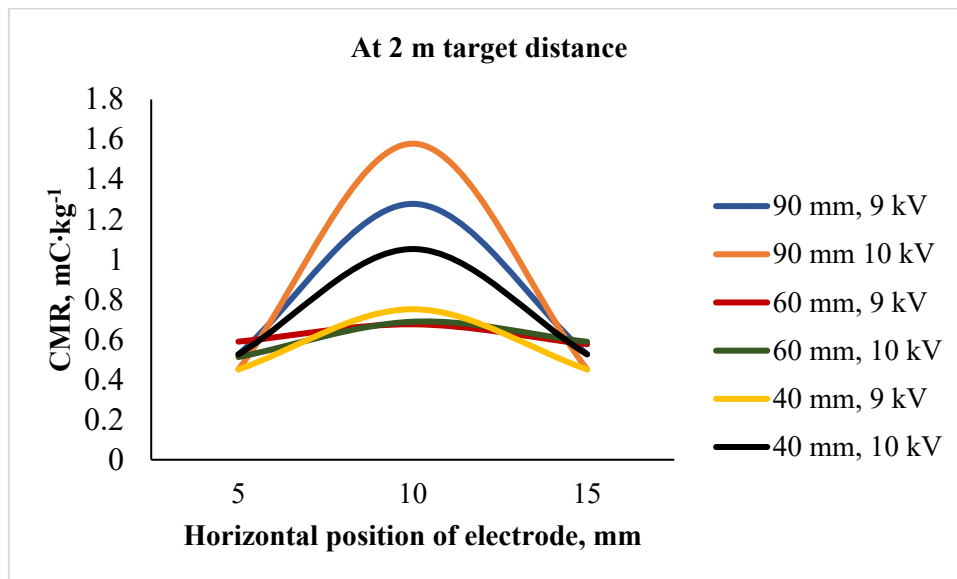


(c)

**Figure 22. Effect of applied electrode voltage on CMR at 2 m vertical distance**



(a)



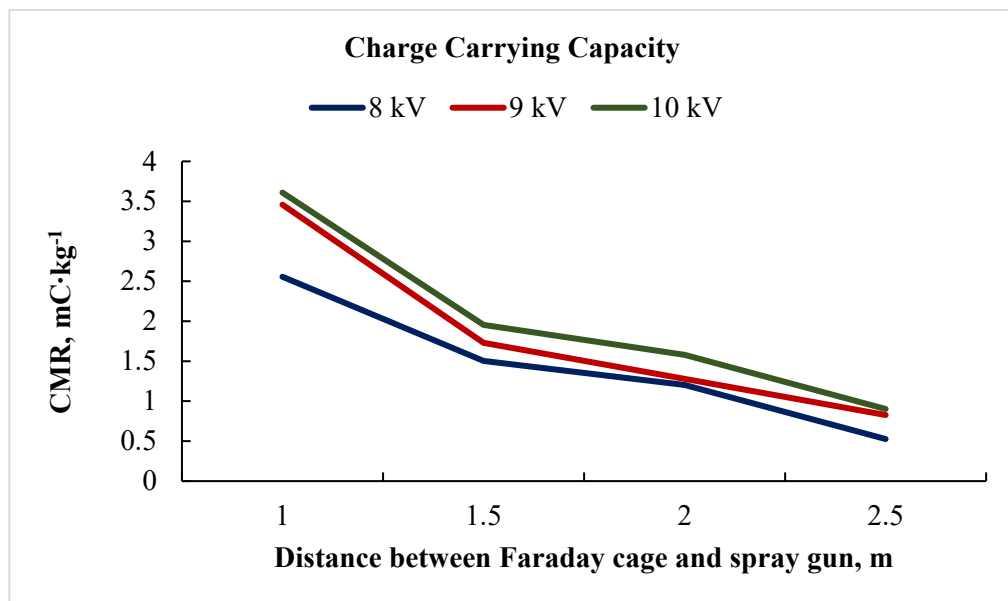
(b)

**Figure 23. Effect of horizontal position of electrode on CMR (a) at 1 m vertical distance (b) at 2 m vertical distance**

#### 4.3.2 Charge carrying capacity of the developed electrostatic charging system

The charge carrying capacity of the electrode-voltage combination was performed by varying the vertical distance between Faraday cage and spray gun. The

current measurement was observed from 0.1 to 4.8  $\mu\text{A}$  for all the electrode-voltage combination at 1, 1.5 and 2 m position. Further increase in the vertical distance shows current reading only for 8, 9 and 10 kV electrode voltages with 90 mm diameter electrode. For 6 and 7 kV electrode potentials, the no current reading beyond 2 m was observed, due to the charge loss along the travel path. With the 40 mm diameter electrode, the droplet reaching points beyond 2 m was found difficult due to loss of droplets as well as air velocity as a result of the reduced cross-sectional area. And for 60 mm diameter electrode, no current reading was observed due to insufficient charge induction to the droplets. The plot of CMR values at different vertical distances of Faraday cage and spray gun was illustrated in the Figure 24. It was observed from the graph that, the CMR was reduced with increase in the vertical distance from 1 to 2.5 m and may eventually become zero on further increase in the distance. This may be due to the charge dispersion as the droplets travels through the atmosphere especially against gravity.



**Figure 24. Charge carrying capacity of 90 mm diameter electrode**

#### **4.3.3 Charging efficiency of the developed electrostatic charging system**

The charging efficiency of the developed electrostatic induction charging was calculated with the Rayleigh's limit of the spray droplet and the maximum CMR

obtained. By considering the CMR readings of all the electrode-voltage combination, it was concluded that 90 mm diameter electrode performs better than the other two electrodes, and the optimum horizontal position was obtained at 10 mm in front of the nozzle tip along the droplet travel direction which was near to the droplet formation zone of the nozzle. The maximum CMR was obtained for 10 kV electrode potential followed by 9 kV electrode potential. From the graphs plotted, it can be concluded that there was only slight variation of most of the observations made at 9 and 10 kV electrode potentials. Considering facts of safety and convenience, it would be better to opt for a lower voltage as both 9 and 10 kV potential showing same results. Hence, Rayleigh's limit,  $q_{\max}$  for spray droplet spectrum of size  $156\text{ }\mu\text{m}$  obtained at 9 kV electrode potential was calculated as  $3.68 \times 10^{-11}\text{ C}$ . The CMR at Rayleigh limit or the maximum theoretical CMR was calculated as  $18.568\text{ mC}\cdot\text{kg}^{-1}$ . The efficiency of the electrostatic spraying system with the practically achieved CMR of  $3.458\text{ mC}\cdot\text{kg}^{-1}$  at an electrode voltage of 9 kV was 18.63 per cent.

#### 4.3.4 Determination of droplet spectrum

The droplet spectrum of the developed air-assisted nozzle, both with and without the electrostatic charging (referred to as ESS ON and ESS OFF, respectively) is outlined in the Table 4 and Figure 25. The observation shows that the VMD was decreasing with increasing the pressure from 3 to  $5\text{ kg}\cdot\text{cm}^{-2}$ . The ESS ON configuration produced a lower VMD compared to ESS OFF across all the three operating pressures. This reduction in droplet size attributed to enhanced atomization caused by the induction of electrostatic charge on the droplets. The induced charge disrupts the natural equilibrium of the droplets, and when the surface charge exceeds Rayleigh limit, it can lead to Coulomb fission. This process causes the droplets to undergo secondary atomization, resulting in a finer droplet spectrum than that achieved with conventional spraying at the same pressure.

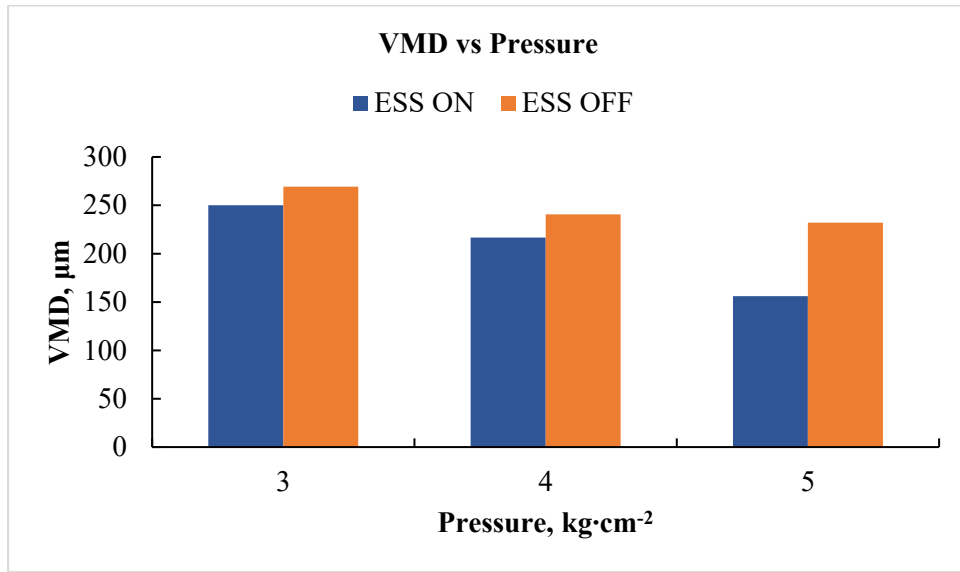
The VMD or  $DV_{50}$  of the spray spectrum when operated at  $5\text{ kg}\cdot\text{cm}^{-2}$  was  $156\text{ }\mu\text{m}$ , while  $DV_{10} = 103.33\text{ }\mu\text{m}$  and  $DV_{90} = 217\text{ }\mu\text{m}$ . Also, the NMD was found to be  $107.49\text{ }\mu\text{m}$ . The uniformity coefficient ( $U_c$ ) was small for higher operating pressures for both ESS ON and OFF. A lower uniformity coefficient of 1.45, indicating a more

evenly distributed droplet spectrum, was achieved at an operating pressure of  $5 \text{ kg}\cdot\text{cm}^{-2}$  in the ESS ON configuration. In contrast, the ESS OFF configuration at an operating pressure of  $3 \text{ kg}\cdot\text{cm}^{-2}$  resulted in a higher uniformity coefficient of 1.72. Similarly, a smaller Relative Span Factor (RSF) of 0.67, which reflects a narrower droplet spectrum with less variation in droplet sizes, was obtained at  $5 \text{ kg}\cdot\text{cm}^{-2}$  with ESS ON. In comparison, the ESS OFF configuration at  $3 \text{ kg}\cdot\text{cm}^{-2}$  exhibited a higher RSF (0.83).

**Table 4. Droplet spectrum with electrostatic charging ON and OFF at different operating pressure**

Parameter	Operating pressure in $\text{kg}\cdot\text{cm}^{-2}$ with ESS ON			Operating pressure in $\text{kg}\cdot\text{cm}^{-2}$ with ESS OFF		
	3	4	5	3	4	5
<b>DV<sub>10</sub>, <math>\mu\text{m}</math></b>	136.00	127.33	103.33	169.67	149.00	118.00
<b>DV<sub>50</sub>, <math>\mu\text{m}</math></b>	250.00	216.67	156.00	269.00	240.67	232.00
<b>DV<sub>90</sub>, <math>\mu\text{m}</math></b>	338.00	274.33	217.00	365.00	326.33	287.00
<b>NMD, <math>\mu\text{m}</math></b>	150.62	128.00	107.49	156.39	151.60	138.00
<b>Uc</b>	1.66	1.69	1.45	1.72	1.59	1.68
<b>RSF</b>	0.81	0.70	0.67	0.83	0.80	0.77





**Figure 25. VMD or DV<sub>50</sub> at different operating pressures**

#### 4.4 FIELD TRIALS ON PERFORMANCE EVALUATION OF THE DEVELOPED PROTOTYPE

The field evaluation of the developed sprayer was carried out at the KCAEFT, Tavanur campus (Plate 7). The sprayer experiments were conducted under both electrostatic charging ON and OFF conditions, while the prototype was operated using the optimized parameters established during laboratory studies and previous field trials.

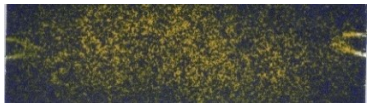



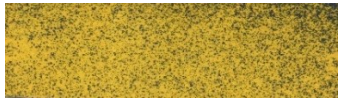

##### 4.4.1 Performance assessment of air -assistance unit

The blower was operated at three different speeds, corresponding to air flow velocities viz. 10, 15, and 17 m·s<sup>-1</sup> with the WSPs placed on the bottom, middle, and upper middle leaves. The Electric Ducted Fan (EDF) was positioned at heights of 1, 1.5, and 2 meters below the canopy, measured from the position of the lowest leaf. During the field trials, it was observed that spraying at the BS1 air velocity (10 m·s<sup>-1</sup>) as ineffective in delivering droplets to the canopy, as the air velocity was insufficient to overcome the downward pull of gravity and air flow resistance. Consequently, subsequent field trials were conducted using air outlet velocities of 15 and 17 m·s<sup>-1</sup>.



**Plate 7. Field evaluation of the developed prototype**

**Table 5. Samples of Water Sensitive Papers collected at different operating conditions of the sprayer**

Sprayer operated from 1 m distance	 Saturated spray (>60%)	 Overspray (44%)
Sprayer operated from 1.5 m distance	 Adequate spray (30%)	 Adequate spray (20%)
Sprayer operated from 2 m distance	 Adequate spray (30%)	 Under spray (6%)

#### *4.4.1.1 Possibility of overspray and under spray*

When the sprayer was operated with the EDF positioned 1 meter below the canopy, the water-sensitive papers (WSPs) in the bottom layers mostly turned blue, indicating a saturated spray with percentage coverage above 50% for both 15 and 17  $\text{m}\cdot\text{s}^{-1}$  air velocities. In the middle layers, the WSPs showed signs of overspray, with coverage percentages ranging from 30 to 40 per cent. Whereas, adequate spray patterns were observed in the upper middle layers.

When the sprayer was operated from a position 1.5 meters below the canopy, adequate spray patterns were achieved across all layers with 17  $\text{m}\cdot\text{s}^{-1}$  air velocity. However, for 15  $\text{m}\cdot\text{s}^{-1}$  air velocity, adequate patterns were observed only in the bottom and middle layers. The upper middle layer exhibited under spray or insufficient spray patterns at 15  $\text{m}\cdot\text{s}^{-1}$  air velocity. When the sprayer was operated from 2 meters below the canopy, middle and upper middle layer showed under spray pattern for both 15 and 17  $\text{m}\cdot\text{s}^{-1}$ . Whereas bottom layer was sufficiently exposed to the spray cloud when operated with 17  $\text{m}\cdot\text{s}^{-1}$  air velocity.

#### *4.4.1.2 Distribution of droplet deposition*

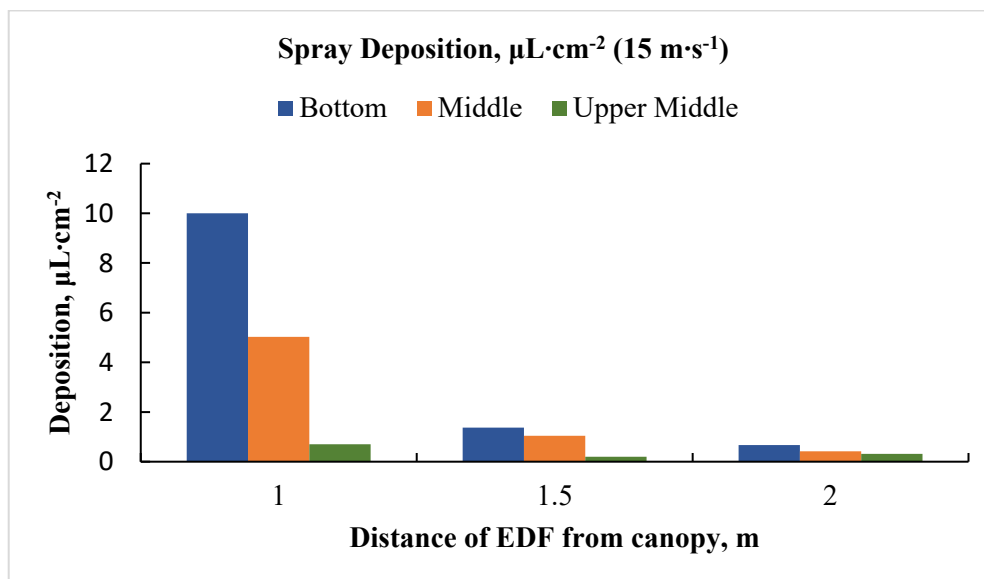
The droplet deposition at two operating velocities is shown in Figure 26. There was a clear trend of decreasing the droplet deposition along the direction of range for all the air outlet velocities. Furthermore, the deposition was decreasing with the lowering the position of EDF. When spraying was conducted from a point 1.5 meters below the canopy, the resulting deposition ranged from 0.8 to 1.9  $\mu\text{L}\cdot\text{cm}^{-2}$  at both operating speeds, which achieved the optimal spray deposition. In contrast, when the EDF was positioned 1 meter below the canopy, the deposition increased by a factor of 4 to 10 in bottom and middle canopy sections compared to that at the 1.5-meter position. Further lowering the EDF to 2 meters resulted in a decrease in deposition at 15  $\text{m}\cdot\text{s}^{-1}$  speed. Whereas at 17  $\text{m}\cdot\text{s}^{-1}$  speed, similar deposition levels as in 1.5 meters was observed.

In all operating air velocities and EDF positions, the leaves located in the lower layers of the canopy exhibit higher deposition rates, as they are more directly exposed

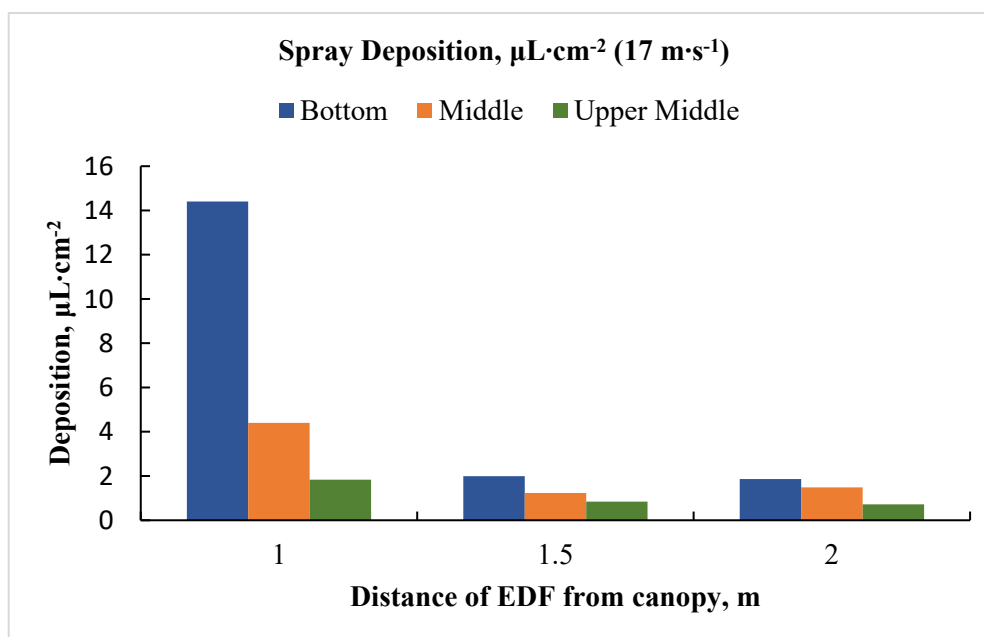
to the spray charge. As the spray cloud penetrates through the canopy, the middle and upper layers receive exposure to the droplets, but to a lesser extent. With the EDF operating at a position of 1.5 meters, the average deposition in the middle layer was measured as 1.232 and 1.045  $\mu\text{L}\cdot\text{cm}^{-2}$  for air velocities 15 and 17  $\text{m}\cdot\text{s}^{-1}$  respectively. Whereas the upper middle layer received less exposure to the droplet charge under same operating conditions. This reduced deposition is due to the longer distance the droplets must travel through the canopy, principally against gravity. The average deposition observed in the upper middle layers at 1.5 m operating position of EDF was 0.884 and 0.201  $\mu\text{L}\cdot\text{cm}^{-2}$  respectively for 15 and 17  $\text{m}\cdot\text{s}^{-1}$  air velocities.

#### *4.4.1.3 Distribution of droplet coverage*

Figure 27 shows the droplet coverage in each layer at different operating position and air flow velocity. There was clear trend of decrease in the droplet coverage with lowering the operating position and increase in the range of spraying. The bottom layers have percentage coverage in the range of 50 to 60 per cent, which were considered as over sprayed as discussed before. The middle layer was observed with droplet coverage in an optimum range for almost all the operating conditions except at 2 m position with 15  $\text{m}\cdot\text{s}^{-1}$  air velocity. However, the upper middle layer was most likely with minimum coverage for all operating condition except at 1.5 m position and 17  $\text{m}\cdot\text{s}^{-1}$  air velocity. An optimum spray coverage in the range of 17 to 25 per cent was observed in all layers of the canopy when the operating conditions 1.5 m position and 17  $\text{m}\cdot\text{s}^{-1}$  air velocity.

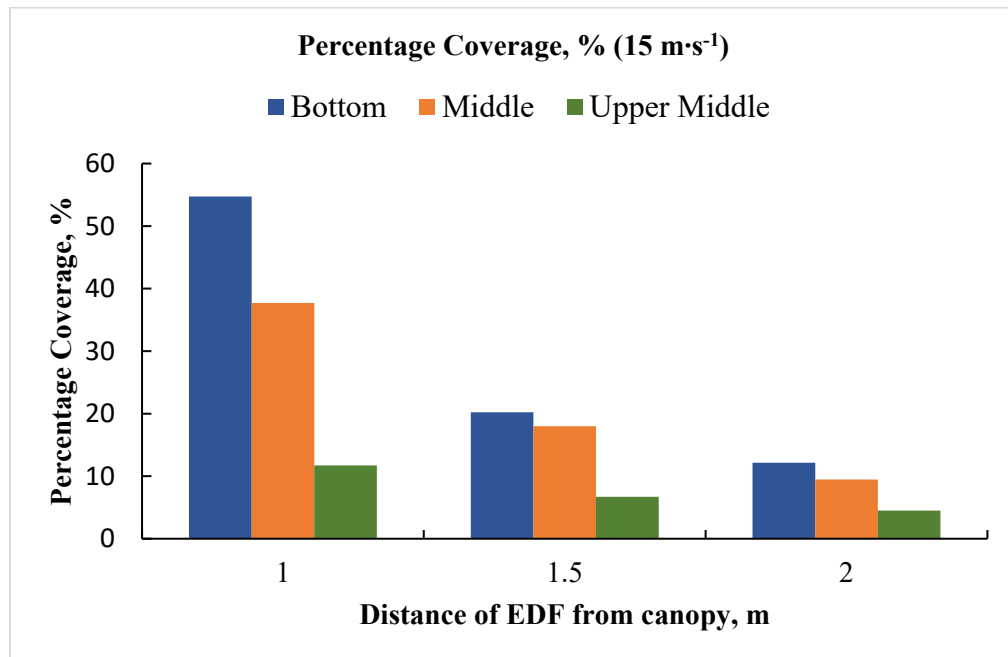


(a)

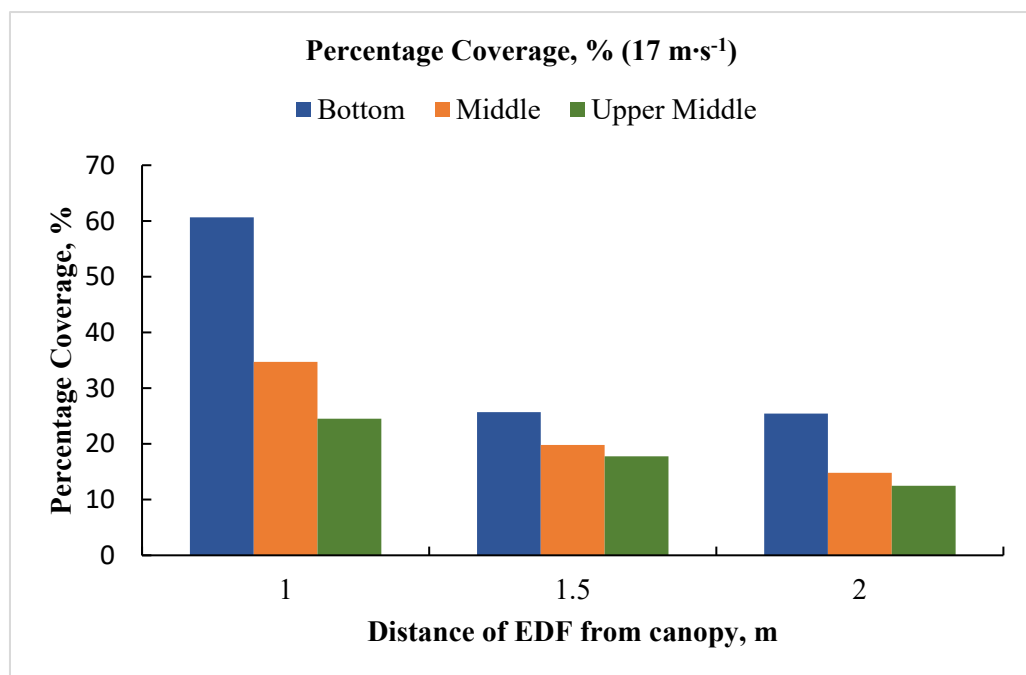


(b)

**Figure 26. Spray deposition at different operating conditions of EDF (a)  $15\text{ m}\cdot\text{s}^{-1}$  air flow velocity (b)  $17\text{ m}\cdot\text{s}^{-1}$  air flow velocity**

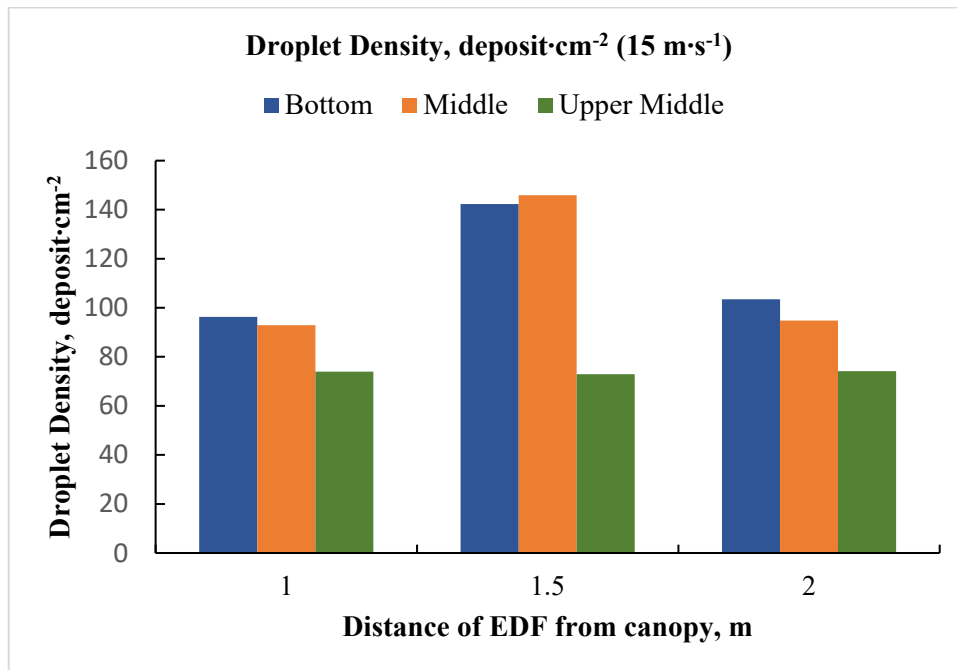


(a)

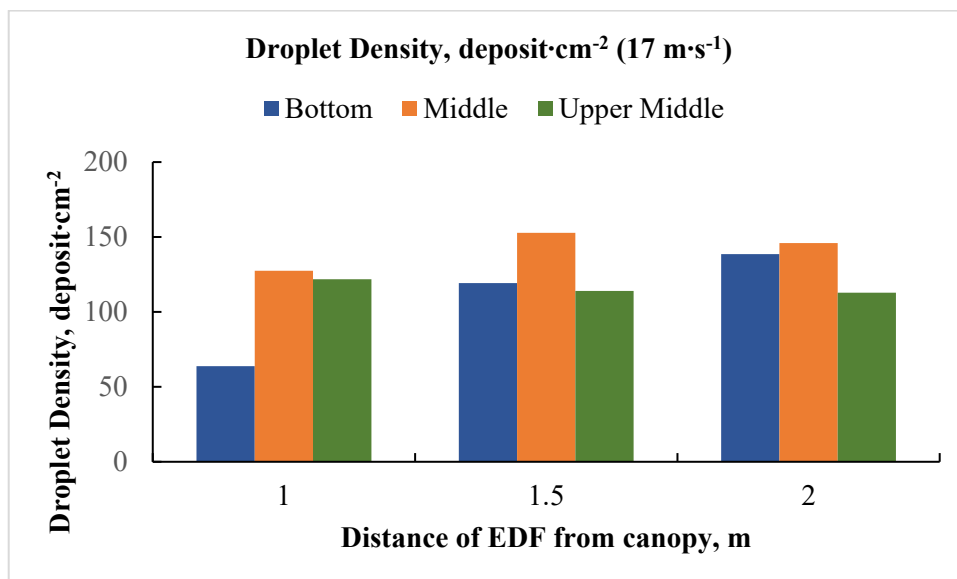


(b)

**Figure 27. Percentage coverage of spray droplets at different operating conditions of EDF (a) 15 m·s<sup>-1</sup> air flow velocity (b) 17 m·s<sup>-1</sup> air flow velocity**



(a)



(b)

**Figure 28. Droplet density at different operating conditions of EDF (a) 15 m·s<sup>-1</sup> air flow velocity (b) 17 m·s<sup>-1</sup> air flow velocity**

#### 4.4.1.4 *Distribution of droplet density*

The droplets per unit area on WSP helps in determining the effectiveness and uniformity of spray distribution. The droplet density for different operating condition is shown in the Figure 28. It was observed that; the droplet density of the middle layer has the maximum droplet density irrespective of the operating conditions. The bottom layer of the canopy has more droplet density compared to the upper middle layer for all the operating conditions. However, droplet density at bottom layer at 1 m operating position and  $17 \text{ m}\cdot\text{s}^{-1}$  air flow velocity contradicts this trend, which has the minimum value of droplet density ( $63.8 \text{ deposit}\cdot\text{cm}^{-2}$ ). The highest value of droplet density was observed as  $152.76 \text{ deposit}\cdot\text{cm}^{-2}$  in the middle layer when the sprayer was operated at 1.5 m position and EDF was operated at  $17 \text{ m}\cdot\text{s}^{-1}$  air velocity.

The middle layer was moderately exposed to the droplet spectrum for all the operating conditions and hence, they have the highest droplet density compared to the other layers. But the bottom layers are directly exposed to the spectrum, which may lead to coalescence of droplets after they get deposited for the canopy. The aggregation of droplet leads to the formation of bigger droplets. The bigger droplets cover larger area and which in turn reduces the droplet deposit per unit area. As the sprayer operated very close to the canopy with higher air outlet velocities of EDF, the chances of coalescence of droplets increases, leads to a minimum value of droplet density.

As the range of spraying increases, the droplet spectrum has to travel long distances to reach the target. The long travel path increases the chance of losses of spray droplets through evaporation as well as drift. This will result in reduced deposit per unit area in the upper middle layers for all the operating conditions.

#### 4.4.2 **Performance assessment of the developed electrostatic sprayer**

The field performance of the developed prototype was assessed in terms of percentage spray coverage, droplet density ( $\text{deposit}\cdot\text{cm}^{-2}$ ) and normalized deposition ( $\text{mg}\cdot\text{cm}^{-2} \text{ leaf} / \text{mg}\cdot\text{cm}^{-2} \text{ leaf ground}$ ). The developed sprayer was operated with the electrostatic charging ON and OFF conditions and the results were compared with the rocker sprayer.



#### 4.4.2.1 Percentage spray coverage

The percentage coverage of droplet abaxial and adaxial side of coconut palm leaves measured using WSPs is shown in the Plate 8 and Figure 29. The highest coverage was observed in the abaxial side of the lower leaves for all the sprayers. The mean coverage in the abaxial and adaxial side of the lower leaves with the ESS ON was observed as 35.1 and 16.5 per cent respectively. The mean coverage for the ESS OFF at abaxial and adaxial side of the lower leaves was recorded as 21.90 and 14.68 per cent respectively. Whereas for the rocker sprayer the same was recorded as 59.62 and 11.28 per cent respectively. The spraying with rocker sprayer resulted in significantly higher coverage in the adaxial side than ESS ON and ESS OFF. As the spray coverage is higher than 50 per cent, spraying with rocker sprayer is considered as ‘overspray’. The spray coverage with ESS ON was observed in the range of 22 to 35 per cent at abaxial surface considered as adequate spray (Michael *et al.*, 2021). In the adaxial side, adequate spray coverage is observed only for lower leaves with ESS ON configuration.

The spray coverage was declining as the spray range increases in the vertical direction for all type of sprayers. Spraying ESS ON results in higher spray coverage in the adaxial surfaces compared to the other two. The adaxial deposition with ESS OFF and rocker sprayer observed due to the dripping of droplets from the upper middle layers and also due to the reverse fall of droplets under the gravity. The results show that spraying with ESS ON has 20.69, 27.23, and 63.95 per cent more adaxial surface spray deposition in the lower, middle and upper middle layers respectively compared to the ESS OFF spraying and 39.05, 22.7, and 84.33 per cent more adaxial surface spray deposition when compared to the conventional rocker sprayer. The statistical analysis indicates (Table 6) that droplet coverage was significantly influenced by both electrostatic charging and canopy height position, with a confidence level of 95%. Details of statistical analysis was given in Appendix VI.



(a)



(b)

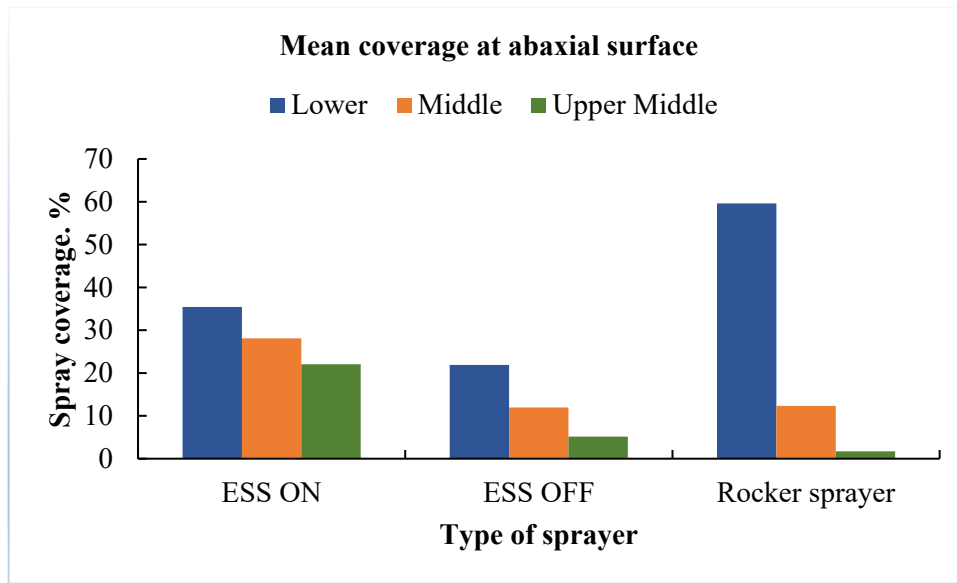


(c)

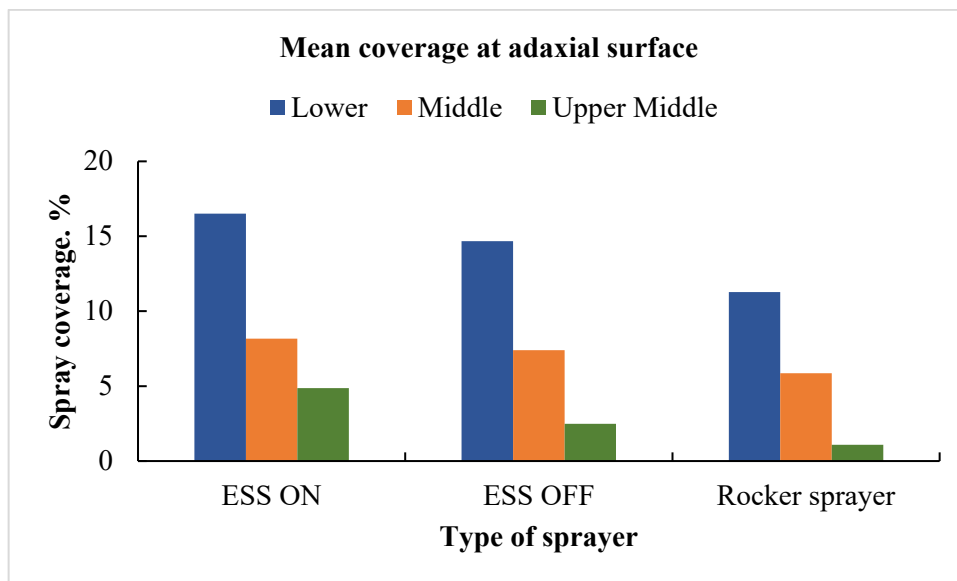


(d)

**Plate 8. Field trials on spray deposition using WSPs (a) ESS ON at abaxial surface (b) ESS OFF at abaxial surface (c) ESS ON adaxial surface (d) ESS OFF at adaxial surface.**



(a)



(b)

**Figure 29. Percentage coverage spray droplets against type of sprayers**

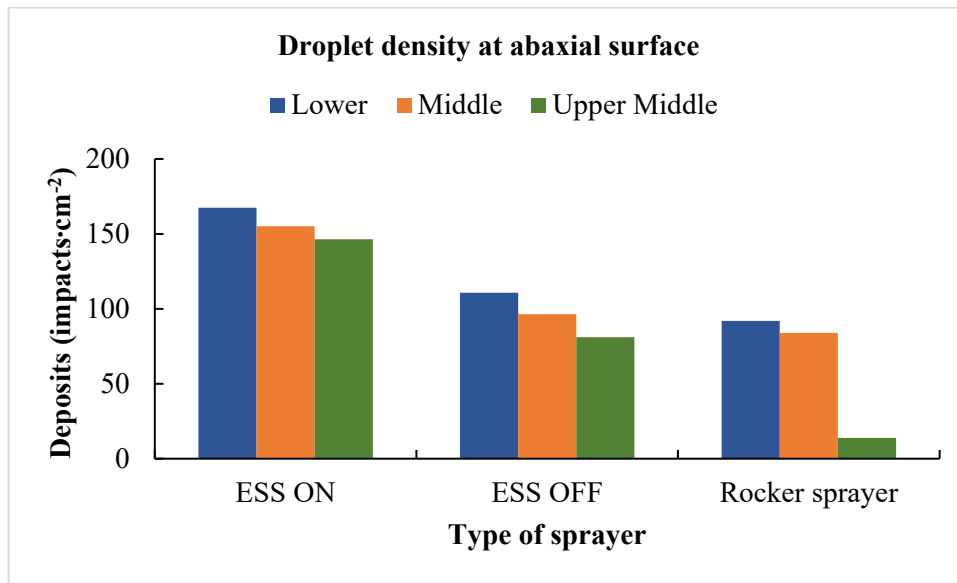
#### 4.4.2.2 Droplet density

Understanding of droplet density of a sprayer is essential for ensuring uniform coverage and maximizing the effectiveness. Figure 30 shows the graphical representation of droplet density in terms of impacts·cm<sup>-2</sup> of the developed sprayer with ESS ON, OFF and rocker sprayer. The highest droplet density was observed for ESS ON spraying for all the three height levels of spraying, followed by the ESS OFF spraying. The least droplet density was observed for the rocker sprayer. A relatively

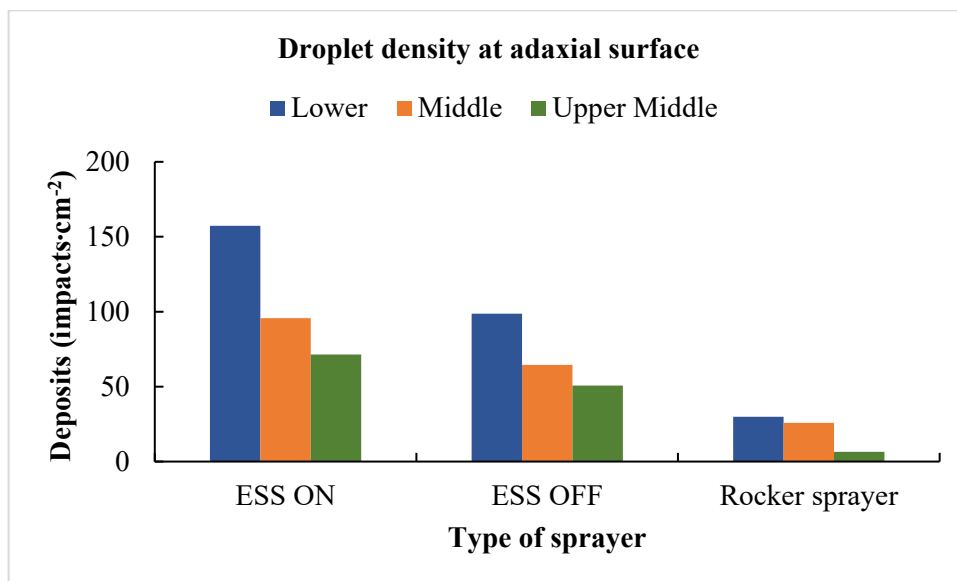
similar droplet density ranging from 146 to 167 impacts·cm<sup>-2</sup>, was observed for ESS ON spraying in lower, middle and upper middle layers at the abaxial surface. The droplet density for ESS OFF spraying at adaxial surface was higher for the lower leaves (157 impacts·cm<sup>-2</sup>) and for the middle and upper middle layers it was recorded as 95 and 71 impacts·cm<sup>-2</sup> respectively. The least droplet density was recorded for the rocker sprayer ranging from 21 to 92 impacts·cm<sup>-2</sup> in the abaxial surface and 6 to 29 impacts·cm<sup>-2</sup> in the adaxial surface. It was concluded that, spraying with ESS ON has 1.81 times more droplet density than rocker sprayer, followed by 1.2 times more than the air-assisted sprayer with ESS OFF. The droplet density was significantly affected by the by the electrostatic charging and the height position within the canopy at a confidence level of 95.0 per cent as shown in the Table 6. The effect electrostatic charging was significantly influencing the droplet density compared to the other two spraying. Whereas the droplet density in the lower and middle layers does not show any significant difference as the p value is 0.094 as given in appendix VII.

**Table 6. Significant effect of the electrostatic system and height position on coverage, droplet density, and deposition at 95.0% confidence level. Significant level: (-) P-Value >0.05; (\*) P-Value ≤0.05; (\*\*) P-value ≤0.01; (\*\*\*) P-Value ≤0.001.**

Main effects	Percentage coverage		Droplet density		Spray deposition	
	Statistical		Statistical		Statistical	
	P value	significanc e level	P value	significanc e level	P value	significanc e level
Sprayer type	3.06E-14	***	9.35E-10	***	3.14E-09	***
Height position	4.25E-19	***	0.002	**	2.9E-13	***
Sprayer type × Height position	1.01E-15	***	.0510	*	0.0052	**



(a)



(b)

**Figure 30. Droplet density against type of sprayers**

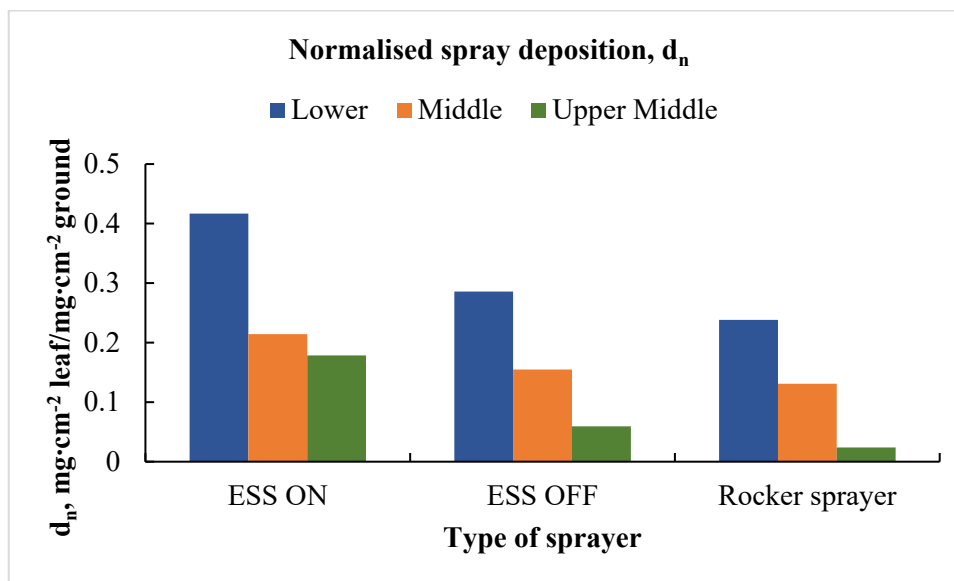
#### 4.4.2.3 Spray deposition

The normalized spray deposition of the developed sprayer with ESS ON and OFF and rocker sprayer was given in the Table 7 and Figure 31. The results shows that the deposit per unit area was decreasing with the range of spraying for all the spraying conditions. The highest deposition was observed on the adaxial surface when sprayed with ESS ON. And the least spray deposition was observed for the rocker sprayer

compared to the other two. Spraying with ESS ON has a spray deposition in the range of 0.20 to 0.42 mg·cm<sup>-2</sup> leaf/mg·cm<sup>-2</sup> ground. Whereas for spraying with ESS OFF, the deposit was observed in the range of 0.07 to 0.30 mg·cm<sup>-2</sup> leaf/mg·cm<sup>-2</sup> ground. It was clearly observed that the electrostatic charging increases the total spray deposition (sum of deposits in all canopy layers) by 1.57 and 1.93 times than air-assisted and conventional spraying respectively. The electrostatic charging of droplets and the height location has significant effect on the spray deposition at a confidence level of 95% as given in Table 6 and appendix VIII. The deposition efficiency was calculated as 69.77 per cent, 43.09 per cent, and 33.86 per cent for the spraying with electrostatic ON, OFF and rocker sprayer respectively. The percentage of spray retained was calculated as 31.59 per cent, 20.09 per cent, and 3.16 per cent for the spraying with electrostatic ON, OFF and rocker sprayer respectively.

**Table 7. Actual and normalised deposit regarding the sprayer type and electrostatic system with standard deviation given in the parenthesis**

Sprayer type	Electrostatic system	Height position	Actual	Normalised
			deposit, d in mg·cm <sup>-2</sup>	deposit, d <sub>n</sub> in mg·cm <sup>-2</sup> leaf/mg·cm <sup>-2</sup> ground
Developed prototype	ON	Lower	3.52 (0.13)	0.42 (0.02)
		Middle	1.95 (0.05)	0.23 (0.01)
		Upper middle	1.67 (0.02)	0.20 (0.01)
Developed prototype	OFF	Lower	2.56 (0.06)	0.30 (0.01)
		Middle	1.42 (0.53)	0.17 (0.06)
		Upper middle	0.56 (0.98)	0.07 (0.12)
Rocker sprayer	-	Lower	2.08 (0.35)	0.25 (0.04)
		Middle	1.18 (0.06)	0.14 (0.01)
		Upper middle	0.41 (0.01)	0.05 (0.01)



**Figure 31. Normalised spray deposit regarding the type of sprayers**

#### 4.4.2.4 *Spray drift*

Plate 9 shows the WSPs placed at 0, 1, and 2 m from the plant canopy when sprayed with ESS ON configuration. Figure 32 represents the spray drift observed at different locations (0 to 4 m) from the plant canopy. When spraying was conducted with the Electrostatic Sprayer System (ESS) turned on, significant spray drift was observed primarily at the point of spraying. As the horizontal distance increased, the drift progressively reduced, eventually becoming negligible at a distance of 2 m. In contrast, when spraying was performed with the ESS turned off, spray drift was detectable up to 3 m. The rocker sprayer exhibited an even greater extent of drift, with spray particles carried up to 4 m. The magnitude of spray drift was significantly higher with the rocker sprayer compared to both the ESS-off and ESS-on conditions. This indicates the effectiveness of the electrostatic system in minimizing drift and enhancing targeted application. It was observed that the spray drift is very negligible with electrostatic charged spray droplets ( $0.87 \mu\text{L}\cdot\text{cm}^{-2}$ ) when compared to the air-assisted ( $10.9 \mu\text{L}\cdot\text{cm}^{-2}$ ) and conventional spraying ( $30.2 \mu\text{L}\cdot\text{cm}^{-2}$ ) as shown in the

Table 8.

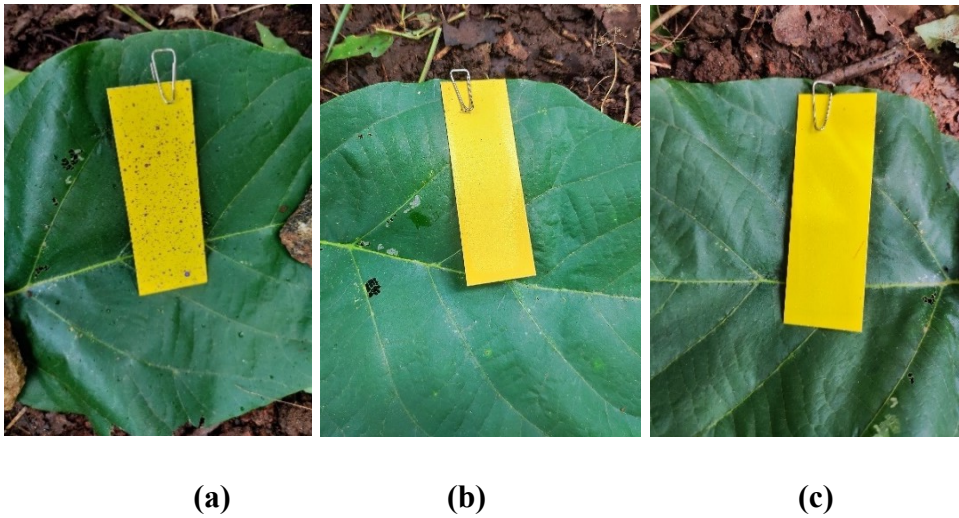


Plate 9. Spray drift observed with developed sprayer with electrostatic charging ON (a) at 0 m from palm canopy (b) 1 m from palm canopy (c) 2 m from plant canopy

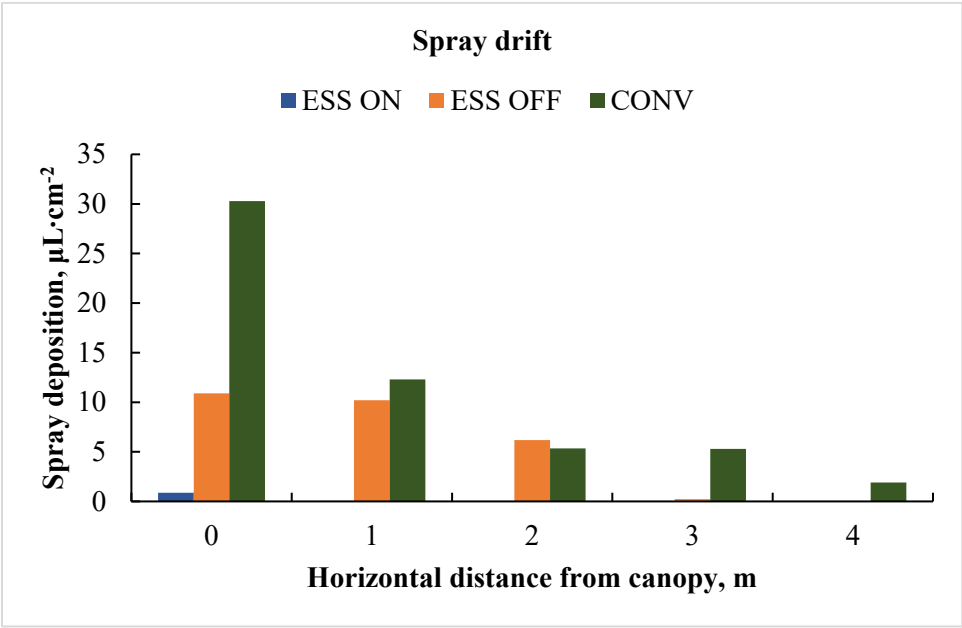
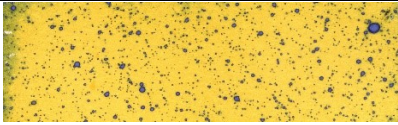

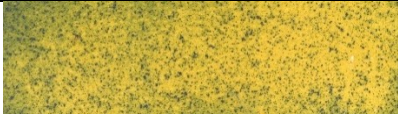

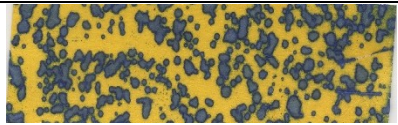
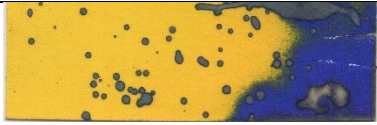


Figure 32. Spray drift at different horizontal locations from the palm canopy



**Table 8. Samples of water sensitive papers collected at different off-target locations when spraying at 17 m·s<sup>-1</sup> air flow velocity.**

ESS ON		
	Spray drift at 0 m	Spray drift at 2 m
ESS OFF		
	Spray drift at 0 m	Spray drift at 3 m
Rocker sprayer		
	Spray drift at 0 m	Spray drift at 4 m

#### 4.5 BIOLOGICAL EFFICACY

Table 9 and Figure 33 shows the effect of different spraying methods on RSW infestation in coconut palms. It is concluded from the results that, spraying with electrostatic charging on has significant effect in controlling the whitefly infestation. Spraying with the spray gun attached to the upper middle end of telescopic pole helps the operator to reach the heights and electrostatic charging aids in the uniform droplet coverage and deposition, leading to a better control of the RSW population compared to the other two spraying. A resurgence of the RSW population was noted 4 to 7 days post-spraying for all the sprayers. Spraying with ESS ON was able to reduce the RSW incidence, severity and RSW live colony per leaflets by 32.76, 64.17, and 74.91 per cent respectively.

Although air-assisted spraying was conducted in a manner similar to electrostatic spraying, it showed lower effectiveness in controlling the RWS population. This could be attributed to reduced droplet deposition and coverage, likely caused by off-target drift. However, air-assisted sprayer yields better control over the RSW population compared to the rocker sprayer. During spraying with the rocker sprayer, a significant portion of the droplets did not reach the target canopy. This may

be due to high off-target drift, leading to inadequate coverage and, consequently, poor pest control.

**Table 9. Efficacy of air – assisted electrostatic sprayer in comparison with air – assisted sprayer, rocker sprayer, and untreated control with the standard deviation given in the parenthesis**

Treatment		Incidence of RSW (%)	Severity of RSW (%)	RSW live colony / leaflet
ESS ON	Pre count	69.32 (6.38)	75.07 (14.51)	16.65 (3.78)
	Post count	46.61 (5.36)	26.32 (4.21)	3.87 (0.92)
	PR	32.76 (7.29)	64.17 (5.03)	74.91 (12.03)
	t value	7.49	7.09	-5.66
	P (<0.05)	0.004*	0.005*	0.01*
ESS OFF	Pre count	62.9 (16.08)	66.17 (5.73)	16.37 (4.62)
	Post count	55.75 (11.80)	46.34 (8.24)	11.31 (1.71)
	PR	10.74 (6.95)	29.81 (11.50)	28.55 (12.67)
	t value	2.61	5.12	4.21
	P (<0.05)	0.079 (NS)	0.014*	0.02*
Rocker sprayer	Pre count	70.91(7.45)	67.40 (4.09)	14.81 (2.71)
	Post count	67.59 (9.93)	58.71 (9.03)	12.43 (1.63)
	PR	4.96 (3.54)	13.11 (9.47)	15.27 (5.75)
	t value	2.89	2.79	2.77
	P (<0.05)	0.060 (NS)	0.068 (NS)	0.069 (NS)
Unsprayed	Pre count	68.58 (10.94)	60.13 (11.80)	18.00 (1.24)
	Post count	80.74 (11.74)	63.58 (11.47)	21.18 (1.28)

PR: Percentage Reduction; \*: significant; NS: Not significant



(a)

(b)

(c)

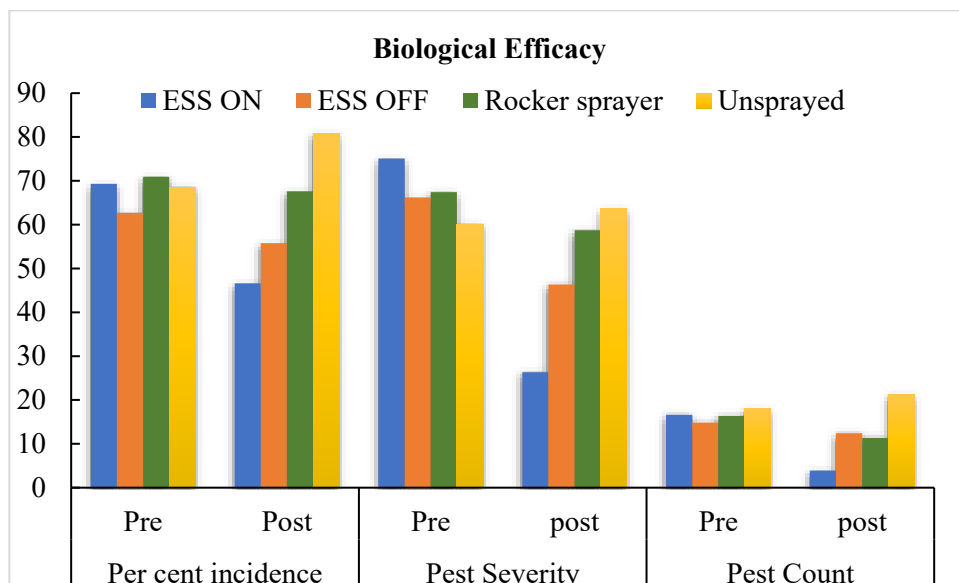


(d)



(e)

**Plate 10. RSW infestation in coconut palm leaf (a) 24 h prior to the treatment, (b) 1<sup>st</sup> day post treatment: ESS ON, (c) 1<sup>st</sup> day post treatment: ESS OFF, (d) 1<sup>st</sup> day post treatment: rocker sprayer, and (e) 4<sup>th</sup> day post treatment: Resurgence of the RSW**



**Figure 33. Impact of different spraying methods in controlling Rugose Spiralling Whitefly (RSW)**

#### 4.6 COST ESTIMATION

The costs of individual components, as well as the total cost of the developed air-assisted electrostatic sprayer for coconut palm is summarized in a Table 10. The total cost of the developed prototype was Rs. 22,120/-. The main components, namely the battery, EDF unit, and spray gun together accounted for approximately 52% of the total cost of the developed prototype. In contrast, the electrostatic charging system costs only 8.7 per cent of the total cost. The commercially available electrostatic sprayers (tractor operated) suitable for orchards costs approximately Rs. 8,50,000/- (Gursukh Agro Works, Ludhiana, Punjab), which is around 38 times higher than the developed prototype. This reduction in the price is achieved without compromising the performance like charge induction, spray deposition, reduced losses etc. The developed system is economically feasible to the Indian farmers without comprising the performance. Unlike the air-blast atomization used in commercial electrostatic, the atomisation of developed sprayer was achieved by a hydraulic nozzle driven by a 12 V DC Double stage diaphragm pump. This design also helped to make the developed prototype more compact and in overall weight reduction of the entire unit. The developed prototype can be easily handled and operated by a single labour.

**Table 10. Estimated total cost of the prototype**

<b>Sl. No.</b>	<b>Components</b>	<b>Quantity</b>	<b>Amount</b>
1.	Lead acid battery, 12 V DC (4 Ah)	1	2100
2.	Rechargeable Li-ion Battery, 3000 mAh	4	1000
3.	Double stage diaphragm pump, 12 V DC	1	1500
4.	Electric Ducted Fan (EDF)	1	7800
5.	Electronic Speed Controller and Servo Consistency Master	1	940
6.	Line Output Transformer (LOPT) 1010A	1	240
7.	Metal Oxide Semiconductor Field Effect Transistor (MOSFET)	1	50
8.	High voltage copper electrode, capacitors and resistors	9	140
9.	PVC Tank, 5 L capacity	1	100
10.	Electrical Insulation, wires, Switches	1 set	600
11.	Hydraulic nozzle, brass fittings and valves, pipe connectors, and pressure gauge	1 set	1750
12.	PU hose tube	12 m	1100
13.	Flexible corrugated tube wire conduit	10 m	550
14.	CPVC Frame and Connectors	1 set	900
15.	Cast nylon for spray gun including laith work	1 set	1500
16.	Miscellaneous		1850
<b>Total</b>			<b>22120</b>

#### 4.6.1 Operational cost

The annual operational cost of the developed air-assisted electrostatic sprayer was calculated for a useful life of 8 years with 250 annual operational hours and detailed in the Table 11. The depreciation was calculated with a salvage value of 5 per cent of the initial cost, and the value obtained as Rs. 2627/- per year.

**Table 11. Operational cost the prototype**

Sl. No.	Particulars	Amount, Rupees
1.	Initial Cost	22120.00
2.	Depreciation at 10 per cent salvage value	2626.75
3.	Interest on investment	1393.56
4.	Taxes, insurance and housing (TIH)	4062.45
5.	Repair and Maintenance	1106.00
6.	Battery recharging cost	209.04
7.	Labour cost	27900.00
8.	Battery replacement cost (cost of additional 2 batteries)	4200.00
8.	Total operational cost per annum ( $\Sigma$ row 2 to 7)	<b>37841.81</b>
9.	Total operational cost per hour	<b>151.36</b>

The interest on the investment was calculated as Rs. 1394/- with an interest rate of 12 per cent per annum. Together depreciation and interest on investment contributes the 12 per cent of the total operational cost. Insurance and shelter (TIH) and repair and maintenance cost were calculated as the 3.5 and 5 per cent of the initial cost respectively. The battery recharge cost per annum was calculated with 250 annual recharge cycles and obtained as Rs. 209/-. The labour cost was determined with Rs. 900/- per day per person, which accounts approximately 83 per cent of the total operational cost.

The operational cost of the developed electrostatic sprayer was calculated to be ₹151 per hour, significantly lower than that of the conventional rocker sprayer, which stood at ₹231 per hour. The developed prototype required approximately 15 minutes to spray a single coconut palm, including setup and transit time between palms, while the

rocker sprayer took about 20 minutes per palm. As a result, the field capacity of the electrostatic sprayer was observed to be 35–40 palms per day, compared to 20–30 palms per day for the rocker sprayer. This analysis clearly demonstrates that the developed electrostatic sprayer offers improved efficiency and cost-effectiveness, enabling greater coverage at a lower operational cost.